Final Technical Report
Dynamical Processes and Forecasts: IFF and Coastal Mediterranean
ONR Grant N00014-94-1-1038
1 September 1994 - 30 November 1994

Allan R. Robinson
Principal Investigator
Gordon McKay Professor of Geophysical Fluid Dynamics
Division of Engineering and Applied Sciences
Department of Earth and Planetary Sciences
Harvard University

This was a project which supported two one-month working visits to the SACLANT Centre, September 9 - October 9, 1994 and October 29 - December 7, 1994. Substantial research collaboration was ongoing between the Harvard Physical Oceanography Group and the SACLANT Applied Oceanography Group, which included two joint cruises to the Iceland Faeroe Front in 1992 and 1993.

During both visits to the SACLANT Centre, Professor Allan Robinson, P.I., interacted with Drs. Alex Warn-Varnas, Arthur Miller, Pierre-Marie Poulain, and Jurgen Sellschopp. The following work statement was developed together with Dr. Alex Warn-Varnas:

1. Perform collaborative work, between SACLANT Centre and Harvard University, on the analysis and the interpretation of the October 1992 and August 1993 IFF (Iceland Faeroe Front) cruise data and the validation of shipboard forecasts conducted with the Harvard University descriptive and predictive system. Provide expertise, guidance, and participate in the writing of publications on: i) Hydrographic Characterization of the IFF, ii) Energetics and Correlations with Data of August 1993 Shipboard Forecasts, iii) Evaluations of Shipboard Forecasts, iv) The Design of an Optimum IFF Forecast System, and v) IFF Predictions Forced by Inflow Conditions Derived from Moorings.

2. Collaborate with SACLANT Centre on the development of a shallow water coastal oceanography program in the Mediterranean. Participate in some aspect of the program.

Both Tasks 1 and 2 were successfully completed. Task 1 resulted in "Real-Time Operational Forecasting on Shipboard of the Iceland-Faeroe Frontal Variability," 1996, *Bulletin of the American Meteorological Society* 72(2), 243-259, which is attached. Three joint Harvard/SACLANT cruises and the design of the Sicily Straits forecast resulted in collaboration initiated in Task 2. The initial work is described in "Real-Time

Regional Forecasting," 1996 in *Modern Approaches to Data Assimilation in Ocean Modelling* (P. Malanotte-Rizzoli, editor), Elsevier Oceanography Series, Elsevier Science, 377-412, which is also attached. The Sicily Straits regional forecast system was successfully used in real time for RAPID RESPONSE 96 and DYNAMIC MIX 96, as attested to in the attached letter (from J. Sellschopp). Results from this exercise will soon be available in a manuscript, "The Atlantic-Ionian Stream," by A.R. Robinson, J. Sellschopp, A. Warn-Varnas, P.J. Haley, W.G. Leslie and C.J. Lozano, which will appear in the Antonio Michelato memorial volume of the *Journal of Marine Systems*.

SACLANT Undersea Research Centre

Address North American Mail to:
CMR 426
APO AE 09613-5000

Viale San Bartolomeo, 400
19138 San Bartolomeo
La Spezia, Italy

8 November, 1996

Application of the Harvard Ocean Prediction System for operational forecast during the military oceanographic survey RAPID RESPONSE 96 and the maritime exercise DYNAMIC MIX 96.

Rapid Response 96 was the first MILOC survey, that was designed for immediate support of a naval exercise with oceanographic and acoustic environmental data. The oceanographic data collection started mid of August, 6 weeks before the navy operation Dynamic Mix 96 took place. Without a means for extrapolation in time, the data set could have been used for broadening the base for climatology in the operation area, but hardly any small scale feature could be expected to persist from August to October.

The participation of the Harvard group in the survey solved the problem of the large time interval between detailed oceanographic measurements and the operational need for accurate data. The Harvard Ocean Prediction System was initialized for the Sicilian Channel with published climatology and data from previous *NRV Alliance* cruises. Rapid Response survey data were assimilated in August on board the ship as soon as they became available. The products which were generated from temperature/salinity profiles were the smoothed and dynamically adjusted temperature and salinity fields and the vector current field. Moreover the dynamic balancing bears in it already the germ for the future development of the hydrographic fields.

Forecasts were started after completion of the first area survey. During the following period new information arrived as satellite images of the ocean surface temperature and as air-borne bathythermography. It was used for comparison of forecasts with reality and it was assimilated into the running system and used for the respective next forecast. In a first attempt for quality assessment, four forecasts of the surface temperature in late August/early September were compared with satellite surface temperature images and the real time analysis of the same days. The quality criterion was the suitable prediction of changes of temperature field features. In nine of twelve cases the tendency was correctly predicted.

The analysis and prediction system was kept running all through the Rapid Response and Dynamic Mix period. Some data from ships were used for updating in addition to the temperature profiles collected by aircraft. Making use of the ocean forecast, it was possible to deliver sound velocity profiles for acoustic modeling of the navy operations areas. Also the drift path of a meteorological buoy was well predicted, the deployment position of which was defined with the knowledge of the main currents in the Sicilian Channel.

The accuracy of modeling results is high if the data used for updating are precise. Care must be taken to remove bad data from the input before they induce unrealistic temperature spots and eddies in the analysis and forecast fields. The range of valid ocean forecasts is restricted by the limited availability of surface fluxes that are part of the atmospheric weather forecast. The Harvard Ocean Prediction System fully met the high expectations. It is the tool needed for updating oceanographic fields by sparse maintaining information. It is highly desired that the Harvard Group takes part in the upcoming Rapid Response 97 survey and again provides participants with ocean analyses and forecasts.

J. Sellschopp
Group Leader, Large Scale
Acoustics & Oceanography Group

Tel: Int. (+39) 187-540-111 / Nat. 0187-540-111 Fax: Int. (+39) 187-524-600 / Nat.0187-524-600 Telex: 271148 SACENT I

Modern Approaches to Data Assimilation in Ocean Modeling
edited by P. Malanotte-Rizzoli

Real-Time Regional Forecasting

Allan R. Robinson,[a] Hernan G. Arango,[a,b] Alex Warn-Varnas,[c,d] Wayne G. Leslie,[a] Arthur J. Miller,[c,e] Patrick J. Haley,[a] and Carlos J. Lozano[a]

[a]Div. of Appl. Sciences and Dept. of Earth and Planetary Sciences, Harvard University

[b]Presently at the Institute of Marine Coastal Sciences, Rutgers University

[c]SACLANT Undersea Research Centre

[d]Presently at Naval Research Laboratory, Stennis Space Center

[e]Presently at Scripps Institution of Oceanography

Abstract

An observational network, dynamical models and data assimilation schemes are the three components of an ocean prediction system. Its configuration for a regional real-time forecasting system proceeds in three phases, based on previous knowledge and experience of the area. In the initial (exploratory) phase, identification of dominant scales (synoptic, mesoscale and submesoscale), processes and interactions is obtained. In the intermediate (dynamical) phase, a clear resolution of the important dynamics and events must be reflected in the nowcasts and forecasts. This is carried out via energy and vorticity analysis (EVA). The third phase is designed to validate the predictive capability of the forecasts. Both qualitative verification and quantitative skill are utilized. At each stage, high quality data sets are required. Observing System Simulation Experiments are essential to the development of the regional ocean prediction system. Initializations and updates are obtained by the fusion of multiple data streams, i.e., the melding of feature models, previous data driven simulations and observations. Nowcasts and forecasts are generated via sequential assimilation combining ship-acquired and sensed remote data. Nested models and nested observations are employed for adequate resolution. The approach is illustrated with recent real-time experiences at sea in the Iceland-Faeroe frontal region, the Straits of Sicily and the Eastern Mediterranean basin.

1. INTRODUCTION

This chapter is concerned with the real-time nowcasting and forecasting of an arbitrary region of the ocean. The region may have both open and coastal boundaries and may be in the deep or coastal ocean or may straddle the shelf break. Ocean forecasting requires both observations and models. The three basic components of an ocean prediction system are: an observational network, a set of dynamical models, and a scheme by which the data are assimilated into the models. The observational network

can consist of a variety of sensors mounted on various platforms. The emphasis in this discussion will be on shipboard forecasts, carried out with data primarily gathered from the ship itself. The work reviewed will be real-time, regional forecasts carried out with the Harvard Ocean Prediction System. Although most of the effort has been directed towards the forecast of physical fields, fully interdisciplinary regional forecasts are now both feasible and important for acoustical, biological, chemical and optical variables.

From a scientific viewpoint, nowcasting and forecasting oceanic mesoscale variability is important to efficiently utilize research resources in the intermittent ocean. Such nowcasts and forecasts are essential for the rapid assessment of a region. General management and Naval operational applications are discussed by Durham and Lewis (1992) and Peloquin (1992) in introductions of the special issues of ***Marine Technology Society Journal*** and ***Oceanography***, respectively, which provide good reviews of the subjects. The real-time shipboard problem is introduced by Robinson (1992). Although mesoscale forecasting research is only about a decade old (Mooers *et al.*, 1986), operational forecasts have been initiated for the Gulf Stream region (Clancy, 1992). This is the region where a relatively good quality data set (Lai *et al.*, 1994) has also been assembled for forecast and simulation validation; preliminary results are presented by Willems *et al.* (1994). Robinson *et al.* (1995a) present mesoscale regional forecasts carried out on shipboard in an operational mode. Lynch (1995) has edited a book, ***Quantitative Skill Assessment for Coastal Ocean Models***, which is generally relevant to ocean prediction techniques.

In this chapter, we describe the nature of the problem of oceanic forecasting, introduce the stages (exploratory, dynamical and predictive; *vid* Section 2) involved in the development of a forecast system and discuss the approach taken for the Harvard ocean prediction system, detail methodology contained within the Harvard system and give specific examples of regional forecasting which have been performed.

The overall development of a regional forecast system is exemplified in the Iceland-Faeroe Front region. The dynamical phase experiment at sea was carried out during October 1992 and the predictive phase forecast experiment took place in August 1993. The Sicily Straits cruise of November 1994 initiated the exploratory phase for that region, chosen for its complex and steep topography and multi-scale circulation features, driven both regionally and remotely. The Eastern Mediterranean cruise may be regarded as contributing to the dynamical stage of the development of a regional forecast system for the entire Eastern Mediterranean basin and illustrates the use of such a prototype system for shipboard forecasting for real-time experimental guidance.

2. NATURE OF THE PROBLEM

The synoptic state of the open ocean is generally dominated by the energetic mesoscale, characterized by the Rossby internal radius of deformation (Robinson, 1983). In the multi-scale synoptic circulation, structures occur over a range of interactive scales, including jet-scale, subbasin-scale, and large-scale. Mesoscale variability is now known to be episodic and intermittent. Mesoscale interactions and synoptical dynamical events occur on space and time scales which are smaller and shorter than the scales for the evolution and propagation of mesoscale features. Such events include rapid

nonlinear cresting of meanders, ring births and reabsorptions, eddy-eddy interactions, streamers and filaments, and are often referred to as submesoscale processes. Event-scales range from O(1–10 km) and O(days), whereas mesoscales range from O(10–100 km) and O(weeks-months). The coastal ocean synoptic state is a multi-scale mix of forced responses and internal dynamical processes. These include wind, tide and boundary forced responses and mesoscale and event-scale processes analogous to those in the open ocean.

Faster and smaller phenomena may also be present and interactive, such as various types of waves, fine- and microstructures and turbulence. The partitioning of scales and phenomena between deterministic and statistical treatments, and between explicit resolution and subgrid scale parameterization must be done partly because of interest and partly because of necessity. Event-scale and submesoscale phenomena of interest require high resolution measurements and dynamical model grids, which are generally impossible to obtain and maintain over the entire region of interest. What is required is nested, high resolution domains, in both the observational network and the dynamical models. Scales smaller than those which can be resolved in the finest grid require subgrid scale parameterization. Forcing mechanisms include surface fluxes of momentum, heat, and fresh water, initial conditions and boundary conditions, which include a representation of larger than regional scales. The nature of the forecast problem is strongly influenced by the relative importance of the response to direct regional surface flux forcing, compared to the evolution via internal dynamics of fields remotely forced in space and time.

Although general processes occur throughout the world ocean, their mix, relative amplitudes and interactions are different in different regions. Regions have their own geometries, topographies and peculiarities. The region chosen for the development of a regional prediction system, may need to be considerably larger than the region of forecast interest for practical purposes, in order to include external influences efficiently. As many regions of the world ocean are still relatively unknown, we will discuss here the development of a regional forecast capability for a relatively unknown region. Better known regions will require less work. Desired forecast purposes (optimal use of research resources, coastal zone management, marine operations (including Naval), etc.), variables, duration and accuracies need to be quantified initially, but must be expected to be iterated and modified as regional predictability is determined. Regional predictability requires accurate estimates of actual ocean states and is influenced by many factors, including the development of instabilities and regional boundaries and boundary conditions.

There are three stages in the development of a regional forecast capability. The first phase is exploratory, the second phase is dynamical, and the third phase is predictive. The exploratory phase is descriptive and kinematical and involves the identification of regional scales, phenomena, processes and interactions. The dynamical phase must be definitive with regard to the determination of synoptic flow structures, regional synoptical dynamical events and interactions, and the elucidation of dynamical processes governing mesoscale evolution and submesoscale events. Dynamical processes such as wave generation and propagation, internal instabilities, dominant external forcings, etc. impose qualitative and quantitative requirements on the design of a regional prediction

system. Nowcasts and forecasts need to be carried out during all three stages. However, during the predictive phase the focus should be on forecast experiments. High quality data sets for forecast initializations, updating and verification are required. Oversampling is necessary in order to determine minimal data requirements for efficient forecasts of desired accuracies.

3. APPROACH

We now describe the general methods utilized for the application of the Harvard Ocean Prediction System (HOPS) to real-time regional forecasts. HOPS is a flexible, portable system whose modularity facilitates efficient configuration for specific applications. Figure 1a presents HOPS in its presently most comprehensive form, with all modules and models attached. Configured for a particular application, the system will generally be less complex. Products are indicated by the rectangles, while models and procedures are indicated by ovals. The 'star modules' represent specific start-up and updating modules (Figure 1b). Lozano *et al.* (1995) discuss the system in detail and Robinson (1995) reviews forecasting applications up to 1993.

From a scientific viewpoint, a central idea for nowcasting and forecasting the multiscale ocean is to attempt to initialize the nowcast or forecast with the best possible estimate of the synoptic state of the system. This contrasts with the approach where a general circulation model may be initialized, e.g., with a mean climatology, and run forward in time in an attempt to develop the regional synoptic state via dynamics with data assimilation. Adequate high resolution and synoptic observations are seldom available for direct initialization so methods have been developed to meld the available synoptic data with synoptic state information from prior observations and dynamical studies. Such information includes prior estimates of the synoptic state of the region from measurements, assimilated observations and realistic regional data driven simulations.

The development of an efficient prediction system for a region thus involves the development of a forecast oriented, historical, synoptical, statistical data base. Statistical models for data reduction and downward extension of satellite data include empirical orthogonal functions in one to four dimensions. Error models, essential for data assimilation, require statistical models for correlation functions, structure functions, and so on. Of particular importance are feature models, i.e., statistical models of typical synoptic structures, a type of structured data model (*vid* Lozano *et al.*, 1995 and Figure 1b). A set of feature models for the dominant circulation structures of the region, kinematically linked via mass-conservation constraints, provides a powerful mechanism for regional initializations and updating. Multiscale linked feature models, developed for the Gulf Stream meander and ring region (Gangopadhyay *et al.*, 1995) have been used together with the primitive equation dynamical model to reproduce the statistics of meander growth and ring formation in the region (Robinson and Gangopadhyay, 1995) and for forecast verification studies (Gangopadhyay and Robinson, 1995). For shelf and coastal oceans, tidal models are necessary; statistical feature models can represent various types of waves, and feature model storms and weather systems can be useful.

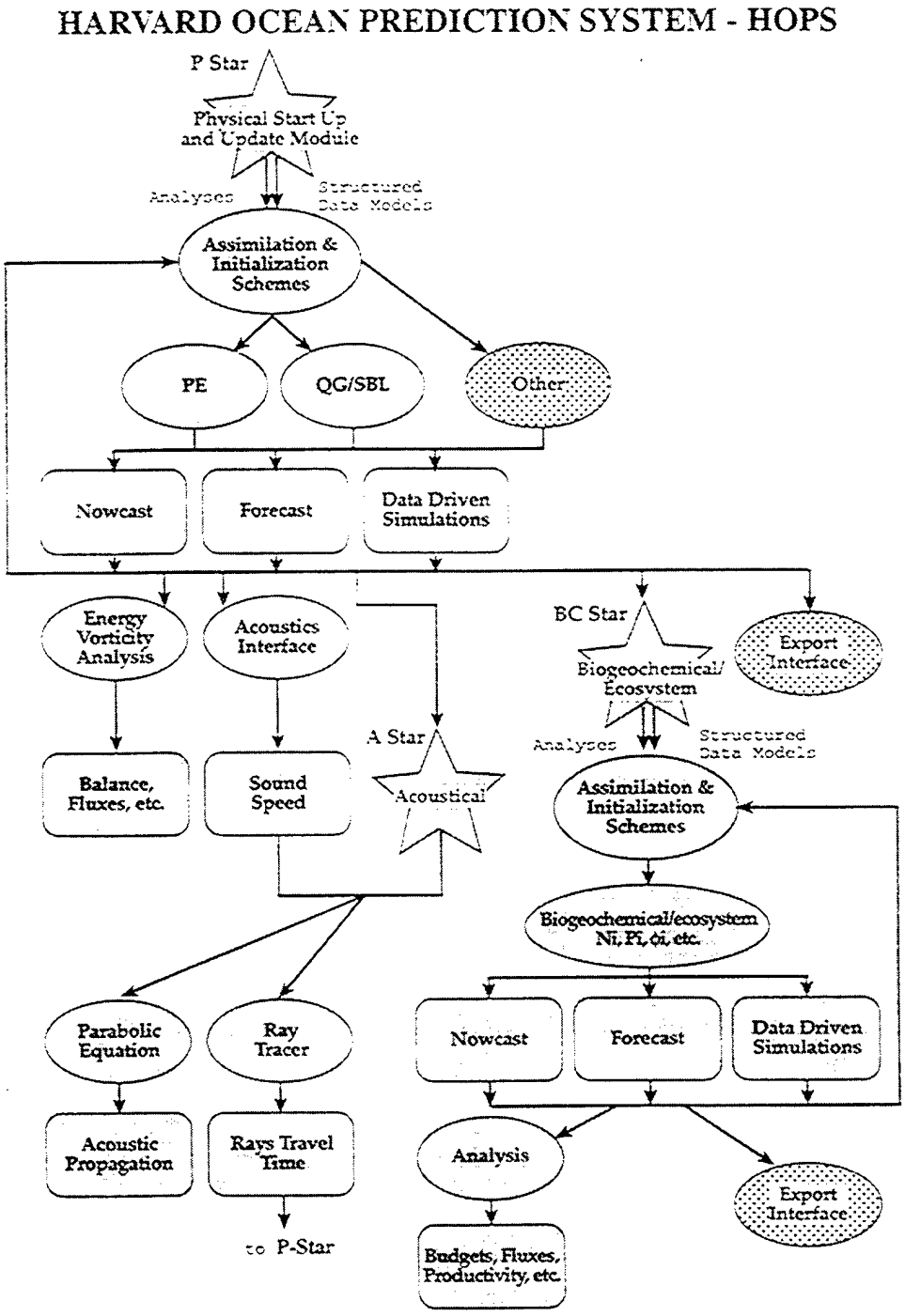

Figure 1a. Schematic of Interdisciplinary Ocean Prediction System. Overview.

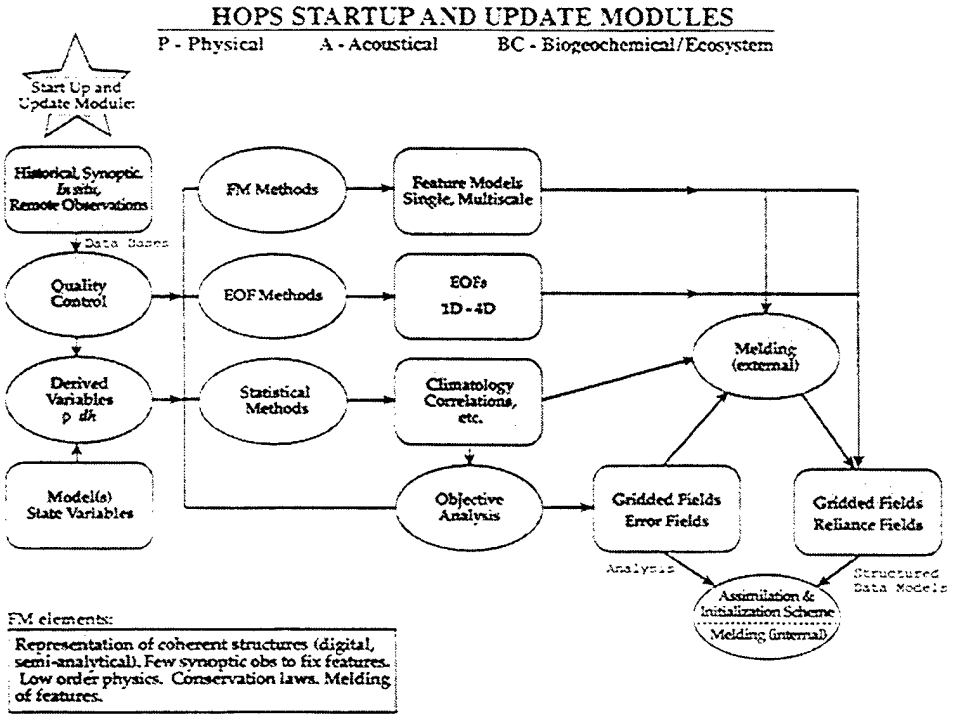

Figure 1b. Schematic of Interdisciplinary Ocean Prediction System. Start-up and update module.

The observational network of the regional forecast system must provide real-time input to nowcasts and forecasts. A mix of platforms and sensors with nested sampling is desirable to provide efficiently information over a range of scales. Coastal areas, ships, aircraft, satellites, moorings, freely floating and roving vehicles are now available as platforms. Dickey (1993) overviews the range of physical, biological and chemical sensors now available.

A variety of data assimilation schemes, based on estimation and control theory, are now available (Bennett, 1992) and methodological research is rapidly progressing (Malanotte-Rizzoli and Tziperman, 1995). For real-time forecasting, a filtering approach is indicated and efficiency considerations are paramount. For applications of the Harvard Ocean Prediction System (HOPS) to real-time regional forecasting, we have chosen a simple, robust optimal interpolation scheme (Lozano *et al.*, 1995). This choice was made not only for efficiency, but also to focus initially on the subtleties of forecast and predictability research rather than data assimilation methodologies.

Verification of a forecast system is an essential task requiring several steps. Prior to commencing forecasts in a specific region, a dynamic model for the region must be chosen and validated. This entails selecting adequately sophisticated physics for the phenomena and scales in the area (e.g., quasigeostrophic equations, shallow-water equations, primitive equations, etc.). The model must then be calibrated and tuned for the environmental, computational, and subgrid scale parameterizations (e.g., the

number of layers or levels, stratification strength, convection and mixing, etc.). The model must be able to capture the dynamics of synoptic events. Verification requires reproducing the statistics of past synoptic events and finally predicting, in real time, new events with qualitative and quantitative skills.

4. SYNOPTIC SHIPBOARD NOWCASTING AND FORECASTING

In this section, we present a methodology to build up and maintain a synoptic description of a region by nowcasting and forecasting on board a ship, primarily utilizing *in situ* data obtained by the ship itself as it moves around the forecast region. The present method of ***sequential updating*** replaces our previous method of ***sequential reinitialization***. In the sequential reinitialization method, a subregion of the entire region is first initialized when sufficient data has been obtained to make a reasonable nowcast and short forecast. With a dedicated research vessel taking hydrographic observations with a mix of CTDs and expendable probes, this is typically one day's (24 hours) worth of data. Then, on each successive day, the model will be reinitialized in successively larger subdomains until the entire domain is covered, at which time the entire forecast domain will be initialized on the central day of the data gathering time interval. In the sequential updating method, when the first subdomain data is available, the entire domain is initialized, using, in the data empty region, elements from the regional historical synoptical data base. On successive days, then, the new subdomain data sets are assimilated via optimal interpolation as they become available. In this way, the entire domain is built up with data being assimilated and evolving as synoptically as possible. As the ship continues to operate in the region, the sequential assimilation procedure is continued whenever sufficient data is obtained over a subdomain to make updating meaningful.

The sequential updating process for the Iceland-Faeroe Front (IFF) is illustrated in Figure 2. The ship is moving from east to west, gathering data along north-south sections separated by 25 km. There are three subdomains and it takes three days to cover the entire area. Initially, the central and western subdomains are initialized by invoking a feature model frontal jet along the climatological mean east-west frontal axis together with climatological mean stratification to the north and south. An objective analysis is made for the entire domain, adding the climatology and feature model data to the eastern subdomain observations. Figure 2 shows the three assimilations and the subsequent forecast via the Primitive Equation model. Figure 2a shows day 1, after the eastern data has been assimilated. Notice the synoptic scale meanders in the eastern part of the front and the contrasting flat feature model front (in its climatological position) to the west. In Figure 2b, another day has gone by and the central domain has been assimilated. The frontal meanders cover more of the domain and synoptic eddies appear. By day 3 (Figure 2c), all the 1992 data has been assimilated. The meanders and eddies now cover the entire region. Finally, an additional four-day forecast is made (Figure 2d). An identifiable, realistic front is present, as are other synoptic scale features.

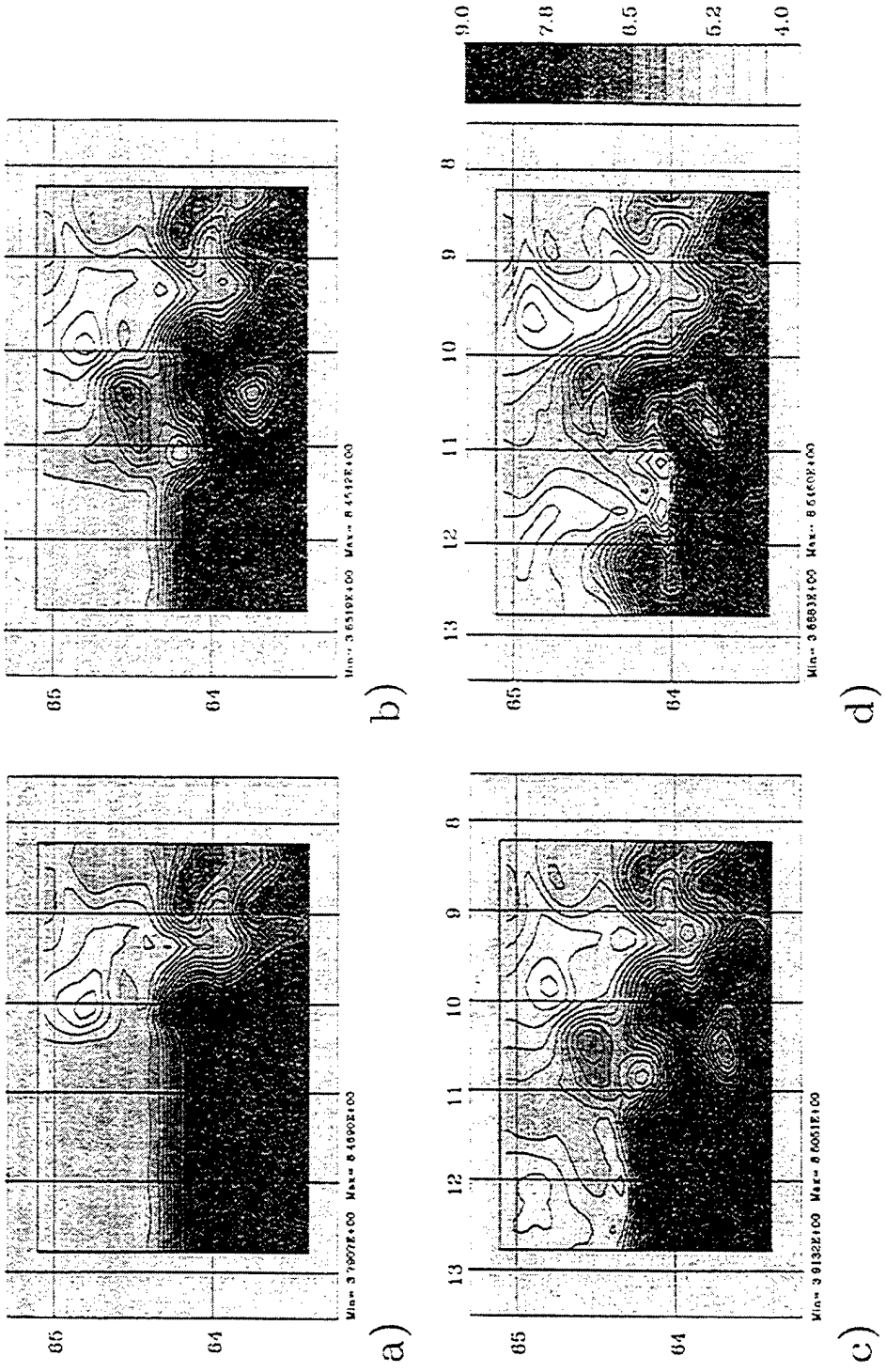

Figure 2. Observational System Simulation Experiment for IFF August 1993 cruise. 25 m temperatures at: a) Day 1, b) Day 2, c) Day 3, d) Day 7.

The illustration of Figure 2 is actually an Observational System Simulation Experiment (OSSE). It utilizes objectively analyzed (OA) data obtained during an October-November 1992 cruise. During the 1992 cruise, data was gathered in a west-to-east pattern. The logistics of current meter recovery and efficient data collection for model initialization and verification, dictated that, in 1993, data would have to be collected in an east-to-west fashion. The OSSE was necessary to validate the details of the data collection and assimilation scheme. The novel aspect of the sampling was moving the ship from east to west against the current. The sampling pattern of Figure 2 was subsequently carried out successfully during August, 1993, as discussed in Section 6.

5. EVALUATION METHODS

Here we describe in greater detail some of the aspects of the methodology which are necessary for the dynamical and predictive evaluation of the regional predictive system. In the exploratory phase of the development of such a system, the procedure is largely descriptive; determining features and process which exist in the region. During the dynamical phase, the strategy of energy and vorticity analysis helps to elucidate an understanding of the regional physics. The final predictive phase necessitates both a qualitative and quantitative assessment of regional predictive ability. Qualitative assessment can be based on measures such as feature location, shape, size, jet axes, eddy center and radii, etc. Specific quantitative skill measures are defined below.

5.1 Energy and Vorticity Analysis

During the development of a forecast capability for a new region, it is essential to understand the physical processes which control the dynamical variability, in order to improve the model physics (e.g., choice of eddy mixing coefficients), the model framework (e.g., the number of layers) and the model geometry (e.g., smoothing of topography). A useful strategy for interpreting the physics of quasigeostrophic (QG) and primitive equation (PE) flows has been energy and vorticity analysis (EVA), developed by Pinardi and Robinson (1986) and Spall (1989) through derivations of the QG and PE energy and potential vorticity equations (and PE divergence equation). Pinardi and Robinson analyzed several selected analytically tractable examples whose energetic and vorticity signatures thereafter form a set of physical benchmarks to which forecasts (or hindcasts) can be compared for insight into the dynamics. The goal is not only to characterize the dynamics of individual events, but also to identify generalizable dynamical processes after many cases have been studied throughout the world ocean.

In order to set the stage for the discussion of energetics of the Iceland-Faeroe Front later in this chapter, we now give a brief introduction to the techniques developed for energetic diagnostics; analogous derivations apply for the vorticity diagnostics which are not presented here. The derivation commences with the quasigeostrophic potential vorticity, written in nondimensional form with characteristic time, T, length, L, depth,

H, and velocity scales, U, as,

$$\frac{\partial}{\partial t}\left(\nabla^2\psi + \Gamma^2(\sigma\psi_z)_z\right) = \alpha J(\psi, \nabla^2\psi) + \alpha\Gamma^2 J(\psi, (\sigma\psi_z)_z) + \beta\psi_x + F_{pqr}. \tag{1}$$

Symbolically (1) can be written as

$$\dot{Q} = \dot{R} + \dot{T} = \Delta F_R + \Delta F_T + \Delta F_P + F \tag{2}$$

where ψ is the quasigeostrophic stream function, $J(\cdot,\cdot)$ is the Jacobian operator, ∇^2 is the horizontal Laplacian operator, $\alpha = TU/L$, $\beta = \beta_0 TL$ and where $R(= \nabla^2\psi)$, $T[= \Gamma^2(\sigma\psi_z)_z]$ and Q are the relative, thermal and dynamic vorticity respectively. The $\dot{(\ )}$ denotes the time rate of change and (ΔF) denotes the advective flux divergence of R, T and βy, the planetary vorticity. The subscripts on the filter have been dropped from (2).

The quasigeostrophic kinetic energy $[K = (u^2 + v^2)/2]$ equation consistent with equations (1, 2) can be written as

$$\frac{\partial}{\partial t}(K) = -\alpha\vec{\nabla}.(\vec{v}K) + \vec{\nabla}.(\psi\vec{\nabla}\psi_t + \alpha\psi\vec{v}.\vec{\nabla}\vec{\nabla}\psi + \beta\psi\vec{v}y)$$
$$+ \frac{\partial}{\partial z}(\Gamma^2\sigma\psi\psi_{zt} + \Gamma^2\alpha\sigma\psi\vec{v}.\vec{\nabla}\psi_z) - \psi_z w + \mathcal{D}_K\ . \tag{3}$$

For ease in subsequent referencing (3) is rewritten using a label for each term in the form:

$$\dot{K} = \Delta F_K + \Delta F_\pi^t + \Delta F_\pi^a + \Delta F_\pi^\beta + \delta f_\pi^t + \delta f_\pi^a - b + \mathcal{D}_K\ ; \tag{3a}$$

or, more briefly, in the form

$$\dot{K} = \Delta F_K + \Delta F_\pi + \delta f_\pi - b + \mathcal{D}_K\ . \tag{3b}$$

The available gravitational energy $[A = \sigma\Gamma^2(\psi_z^2)/2]$ equation is

$$\frac{\partial}{\partial t}(A) = -\alpha\vec{\nabla}.(\vec{v}A) + \psi_z w + \mathcal{D}_A\ , \tag{4}$$

or

$$\dot{A} = \Delta F_A + b + \mathcal{D}_A\ . \tag{4a}$$

where again the symbols in (4a) correspond to the terms in (4). The nondimensional parameters are $\Gamma^2 = f_o^2 L^2/N_o^2 H^2$ and $\sigma = N_o^2/N^2(z) = -N_o^2/g(\partial\bar{\rho}/\partial z)$. In the above, f_o, and β_o are representative values of the local rotation rate and its latitudinal gradient.

The symbols representing the terms in (3, 4) are ΔF_K, the horizontal KE advective working rate; ΔF_π, the horizontal pressure working rate, which is further broken up into three terms, ΔF_π^t, that due to acceleration of the geostrophic velocity, ΔF_π^a, that due to advection of the geostrophic velocity, and ΔF_π^β, that due to Coriolis acceleration;

δf_π, the vertical pressure working rate, which is further broken up into two terms, δf_π^t, the vertical pressure energy flux divergence due to time changes in density, and δf_π^a, the vertical pressure energy flux divergence due to horizontal advection of density; b, the buoyancy working rate; and ΔF_A, the horizontal AGE advective working rate. The $\mathcal{D}_{K,A}$ are dissipation terms in the energy equations arising from the Shapiro filter operation on the vorticity.

A suite of simple solutions of the quasigeostrophic equations was examined to gain physical insight into expected spatial and temporal relationships among the dominant terms in (3, 4). The analysis included a simple baroclinic Rossby wave, the eddy baroclinic instability problem and a particular barotropic instability example. The Rossby wave example exhibits the benchmark interplay among the terms in (3, 4), with the two instability solutions revealing perturbations about that basic wave-like state. Simple propagation involves a periodic exchange of K and A through b, and the instability signals are usually asymmetries of the large propagation noise. In the eddy baroclinic instability model (pure vertical shear), buoyancy work is negative definite in the mid-depths of the water column, indicating a transfer of energy from AGE to KE. The source term for the AGE is the energy of the shear flow, arising through ΔF_A. Besides the forcing through buoyancy coupling at mid-depths, the KE equation is driven near the surface and bottom through vertical exchange processes, δf_π in the baroclinically unstable case. The term δf_π drains the KE at mid-depth and drives the KE at the top and lower boundaries. In the barotropic instability model (pure horizontal shear) that they selected, the AGE equation is inconsequential. The dominant source term in the KE equation is ΔF_κ, corresponding to a Reynolds stress effect drawing energy from the mean shear. Developing additional analytical or numerical basic examples to add to this list (e.g., topographic waves, radiating instabilities) is an important future direction for EVA.

Dynamical analyses of simulations and forecasts are required to understand processes. These are carried out via term-by-term balances. Consistent schemes have been developed for analyzing the potential vorticity, kinetic energy and available gravitational energy for the quasigeostrophic equations (Pinardi and Robinson, 1986) and the vorticity, divergence and energies for the primitive equations (Spall, 1989). QG dynamical studies have been carried out for the California Current (Robinson *et al.*, 1986), the North Atlantic mid-ocean eddy field (Pinardi and Robinson, 1987), the Gulf-Stream (Robinson *et al.*, 1988) and the Eastern Mediterranean (Golnaraghi, 1993a,b) and the Iceland-Faeroe Front (Miller *et al.*, 1995a,b). PE studies have been carried out in the mid-ocean eddy field (Spall, 1989) and the Gulf Stream (Spall and Robinson, 1990).

5.2 Verification and Skill Assessment

A quantitative validation of forecast skill is highly desirable, but the difficulty of acquiring sufficient oceanic data for both initialization and validation means that convincing demonstrations of mesoscale ocean forecast skill are rare. Measures of forecast

skill we use are the pattern correlation coefficient,

$$\mathrm{PCC} \equiv \frac{< \psi_p' \psi_o' >}{(< \psi_p'^2 >< \psi_o'^2 >)^{1/2}} \tag{1}$$

and the normalized root-mean-square error,

$$\mathrm{NRMSE} \equiv \frac{< (\psi_p - \psi_o)^2 >^{1/2}}{< \psi_o^2 >^{1/2}} \tag{2}$$

where ψ_p is the predicted variable (e.g., stream function), ψ_o the observed variable (e.g., dynamic height scaled to stream function), the primes denote removal of the spatial mean, and the angle brackets denote averaging over the specified horizontal area. The forecast variable ψ_p will apply either to the dynamical prediction or to using persistence of day 0 as the predictor.

Measures of quantitative dynamical forecast skill must first be gauged relative to persistence of day 0. Once that baseline is demonstrated, forecast models can be compared relative to each other. To attach statistical confidence to measurable skill of a forecast model, one would need many data sets with adequate initial and verifying data, and this is presently very difficult to realize for oceanic forecasting (Willems *et al.*, 1994; Lynch, 1995).

6. THE ICELAND-FAEROE FRONT

The Iceland-Faeroe Front (IFF) is located between Iceland and the Faeroe Islands in a region where the ocean bottom rises to within 400 m of the surface. The front forms the confluence of the warm saline North Atlantic water mass and the cold low salinity Arctic water mass. Strong currents and sharp temperature gradients are found in this area. A composite picture of the current structures has emerged that shows a flow along the frontal area with inflow from the North Atlantic along the southeastern Icelandic shelf. Some inflow of Arctic-type water occurs along the northeastern Icelandic shelf and merges with the North Atlantic water inflow at the frontal location off Iceland (Peggion, 1991). In the frontal region, a high degree of mesoscale and event-scale dynamical activity exists. Frontal meanders, cold and warm eddies are present. Atmospheric cooling, mixing of the upper ocean, internal tides and internal waves occur.

6.1 Forecast Experiments

This has been a particularly successful region for executing the previously described 3-phase strategy of regional forecast system development (Section 2). The forecast experiment cruises were carried out cooperatively by Harvard and SACLANT scientists aboard the *R/V Alliance* in October 1992 (Arango *et al.*, 1993), and August 1993 (Robinson *et al.*, 1994), but significant work had been achieved before those dates, in tuning both quasigeostrophic (QG) and primitive equation (PE) models for specific

application to that region. Denbo and Robinson (1988a, b) had shown that QG physics were sufficient to capture many aspects of the natural variability of the IFF and a suitable set of model environmental parameters had been identified.

The October 1992 cruise to the IFF was designed to provide a hydrographic data set geared specifically towards initialization and validation of a forecast. It turned out that poor weather limited the data set in two ways. First, the initialization survey required 5.5 days to complete and therefore was not synoptic. Second, the validation survey was necessarily limited to a single criss-cross track over the model forecast region, rather than a complete resurvey of forecast fields. Nonetheless, the data set proved essential for tuning the dynamical models, for demonstrating qualitative forecast skill in the region, and for identifying underlying dynamical processes (Miller *et al.*, 1995a).

During the August 1993 cruise to the IFF, the tuned QG model and a primitive equation model, capable of handling steep and tall topography, were both used in real-time forecasts. Real-time, shipboard nowcasts and forecasts were used to define and predict regional structures and provide experimental guidance. As fine weather prevailed during the expedition, the forecasts were able to be validated quantitatively for skill in two separate initial states, i.e., at the beginning and the middle of the cruise. Both the QG model (Miller *et al.*, 1995b) and the PE model (Robinson *et al.*, 1995a) forecasts showed significant real-time quantitative forecast skill, beating the persistence of day-zero conditions to at least 3 or 4 days, with strong events occurring. A striking, deep-sock meander developed from an initial simple, gentle meander pattern. A PE model forecast (executed post-cruise in forecast mode with an improved model over that used at sea) for 25 m depth temperature shown in Figure 3a, exhibits submesoscale features that corresponds well to those observed in the satellite SST map (Figure 3b), which was obtained on a rare clear day. Quantitatively the at sea forecast was comparable but slightly better.

The observations and PE forecasts are summarized in Figure 4 in terms of the temperature fields at 125 m. Figures 4a, b, and c are objective analyses on the central day of three day regional surveys. The first and last were complete surveys, and the intermediate survey focussed on critical features with a zig-zag sampling pattern. Note that the inlet position of the front on the western boundary is nearly stationary throughout the experiment. On August 15 (Fig. 4a), the IFF was oriented eastward in a distinct meander pattern with a crest at about 11.5°W longitude and a trough at about 11°W. In the east, the flow broadens and bifurcates around a pair of eddies only partially contained within the domain. The upper frontal system evolved rapidly and changed qualitatively between each survey. By 19 August (Fig. 4b), the meander had disappeared and the straightened frontal stream had shifted to a southeastward orientation in the western domain and a northeastward orientation in the eastern domain. However, only three days later, on 22 August (Fig. 4c), the dominant synoptic feature was the large, cold intrusion, or deep sock meander, which had developed in the center of the domain (Miller *et al.*, 1995b; Robinson *et al.*, 1994, 1995a).

Nowcasts and forecasts were carried out using the sequential updating method initialized in the manner of the OSSE of Figure 2. The nowcast of Fig. 4d and the forecasts of Figs. 4e,f utilize data from the first 3-day survey only. Figure 4g has been updated with the intermediate survey data and Fig. 4h is the resultant forecast. Note,

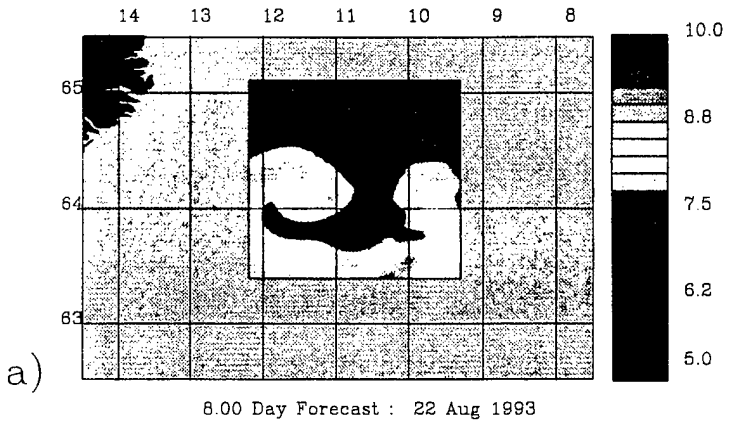

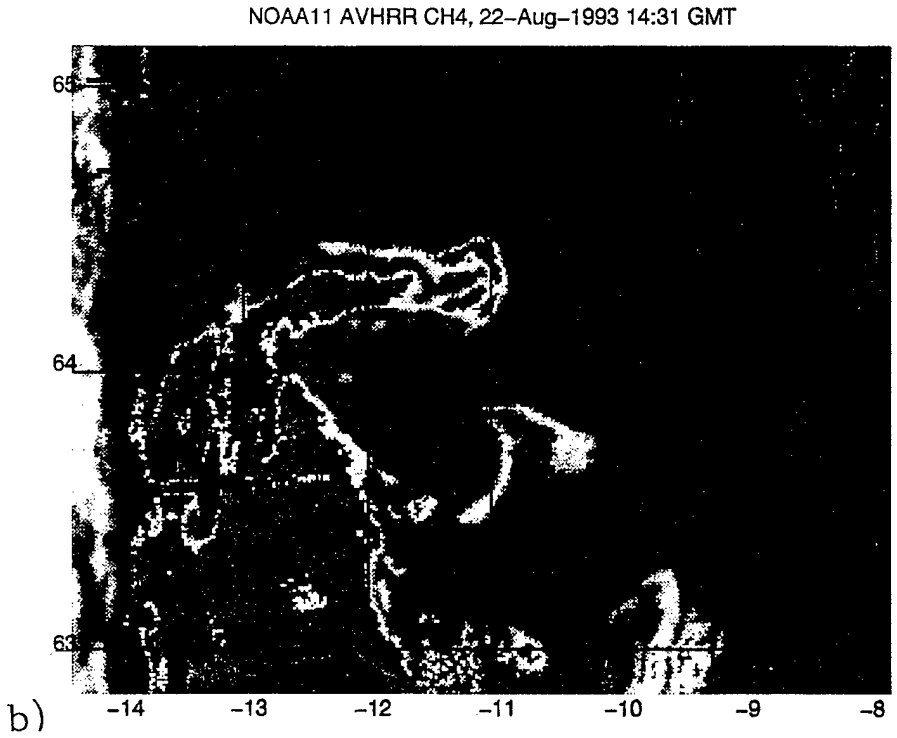

Figure 3. a) Primitive equation model 25 m temperature forecast for 22 August 1993. b) Sea-surface temperature from satellite IR for the same date. Modeling domains is outlined on b).

importantly, that dynamics successfully accomplish the straightening of the jet and its southward orientation (Fig. 4e) and also predict the deep sock meander.

The day-2 nowcast, Fig. 4d, has assimilated, via intermittent optimal interpolation in three daily cycles (sequential updating - Section 4), the entire initialization survey data set. It represents a field estimate in which day-2 synoptic data has been assimilated synoptically at the central day, and as a result of previous assimilations in the cycle, the data dynamically adjusted, dynamically interpolated, and dynamically extrapolated by the model. It should be compared with the objective analysis for the central day of the survey Fig. 4a. Although a time-dependent OA was used, since every region of the domain was sampled only once, the full domain maps for August 14, 15, 16 are essentially identical to the central day map (Fig. 4a). What differs from day to day are the maps of expected error of the analyses. The OA (Fig. 4a) and nowcast (Fig. 4d) estimates are very similar but there are significant differences. In the nowcast, the meander crest has smoothed and the trough has weakened and propagated westward. We believe that these dynamical adjustments are real and that the nowcast estimate based on synoptically assimilated data melded with dynamics provides the most realistic picture of the frontal system.

6.2 Event Dynamics

The dynamics of the flow fields involved in the occurrence of the major synoptic events, such as rapid shifts and deep meandering, have been studied. In each of the two cruises to the IFF, a strong internal instability event occurred. During October 1992, a cusp-shaped cold intrusion developed along an east-west oriented frontal current (Miller *et al.*, 1995a). During the August 1993 IFF cruise, a gentle meander pattern first straightened and shifted to the southeast, which was followed by the development of the deep sock meander (Figures 4a-b).

The instability processes which control current variations in the Iceland-Faeroe front (IFF) have been studied by Miller *et al.* (1995a,b) using the EVA diagnostics. Three mesoscale events occurred during two forecast expeditions to the IFF, and these were modeled successfully in their QG forecasting experiments. For each of the three synoptic events, a diagnostic breakdown of the AGE and KE equations revealed that energetic conversion processes are at work which are consistent with those that occur in a simple model of baroclinic instability (the eddy problem discussed in Section 5.1). The source term for barotropic instability was very small and inconsequential during these three events. Somewhat surprisingly, the baroclinic instability mechanism occurs for each of the three mesoscale events, suggesting the predominance of the mechanism, even though the spatial structure of the current variations differ considerably from case to case. A schematic of the basic energetic exchange processes which occurred for those three IFF synoptic events is sketched in Fig. 5, mapped in Fig. 6, and discussed more thoroughly in the next paragraphs.

The specific details of the energetic exchange processes are as follows. In October 1992 a cold tongue intrusion of the IFF grew as a wave-like meander on an east-west oriented frontal current. The EVA energetic breakdown showed that AGE was

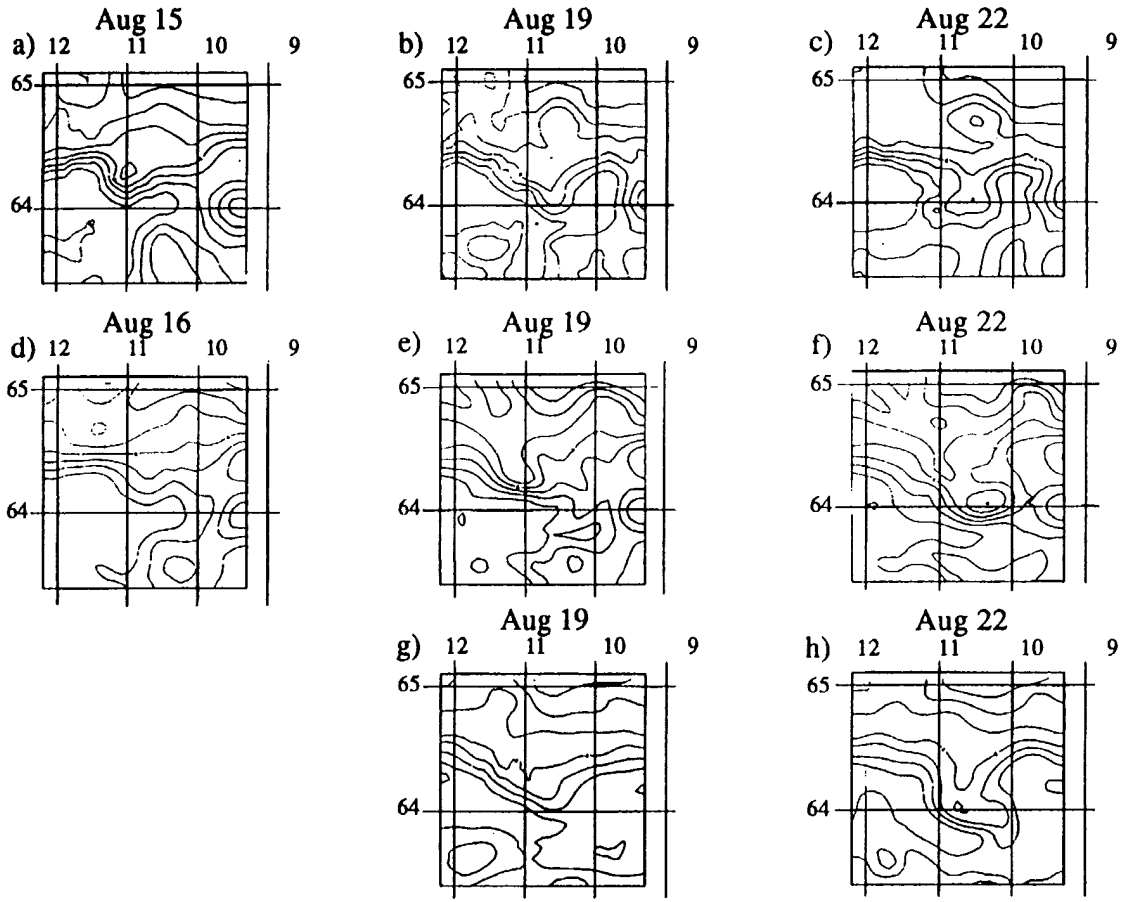

Figure 4. IFF primitive equation model forecast validation. 125 m temperatures. Contour interval is 1°C. a), b) and c) are objective analyses for Aug. 15, Aug. 19 and Aug. 22, respectively. d), e) and f) are forecast days 0, 3 and 6 for a forecast which does not contain the updating data from Aug. 19. g) and h) are days 3 and 6 for a forecast which contains the updating data from Aug. 19.

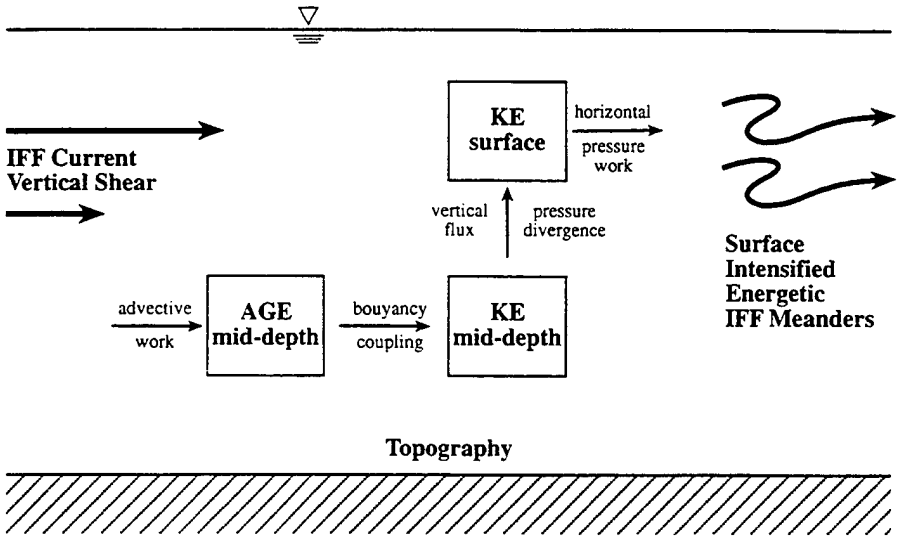

Figure 5. Schematic of energy processes in Iceland-Faeroe Front region.

converted to KE in the mid-depths of the water column from where it was transferred upward into the near-surface KE field yielding the surface current field associated with the cold tongue intrusion. The whole process required roughly 3-4 days to develop indicating the rapid exchanges of energy which can occur in this region (Miller *et al.*, 1995a).

A similar sequence of energetic transfers prevailed during the two synoptic events observed and forecast during August 1993 (Miller *et al.*, 1995b). In these two cases, however, the growing unstable perturbations were not wave-like, but rather occurred as localized disturbances which developed over 3-4 day time scales on a convoluted IFF current. From an initial meandering IFF current, the dynamics shifted the current to a southeastward flowing state through baroclinic instability processes similar to those described above. Likewise, the southeastwardly flowing initial current developed into an intense hammerhead intrusion along the IFF via the same dynamical process, the which is schematized in Fig 5, corresponding to day 3 (August 23, 1993) of the dynamical QG forecast. The velocity field at 250 m depth (Fig. 6a) is related to the hammerhead pattern in sea-surface temperature seen near the surface. At mid-depth (250 m), the advective working rate in the available potential energy (AGE) equation (Fig. 6b) indicates that a net transfer of energy from baroclinic shear flows occurs at the leading edges of the developing hammerhead. Mirroring that effect in sign, the net buoyancy working rate (Fig. 6c) shows that this energy is drained from the AGE and converted to kinetic energy (KE) in the mid-depths of the water column. The vertical pressure-working rate (Fig. 6d) reveals a net upward transfer of KE towards the vigorous current field of the surface layers. These processes of IFF current variability correspond remarkably well to the basic energy exchange patterns diagnosed from the very simple Eady baroclinic instability problem.

The surface-intensified nature of the baroclinic instability mechanism evidently

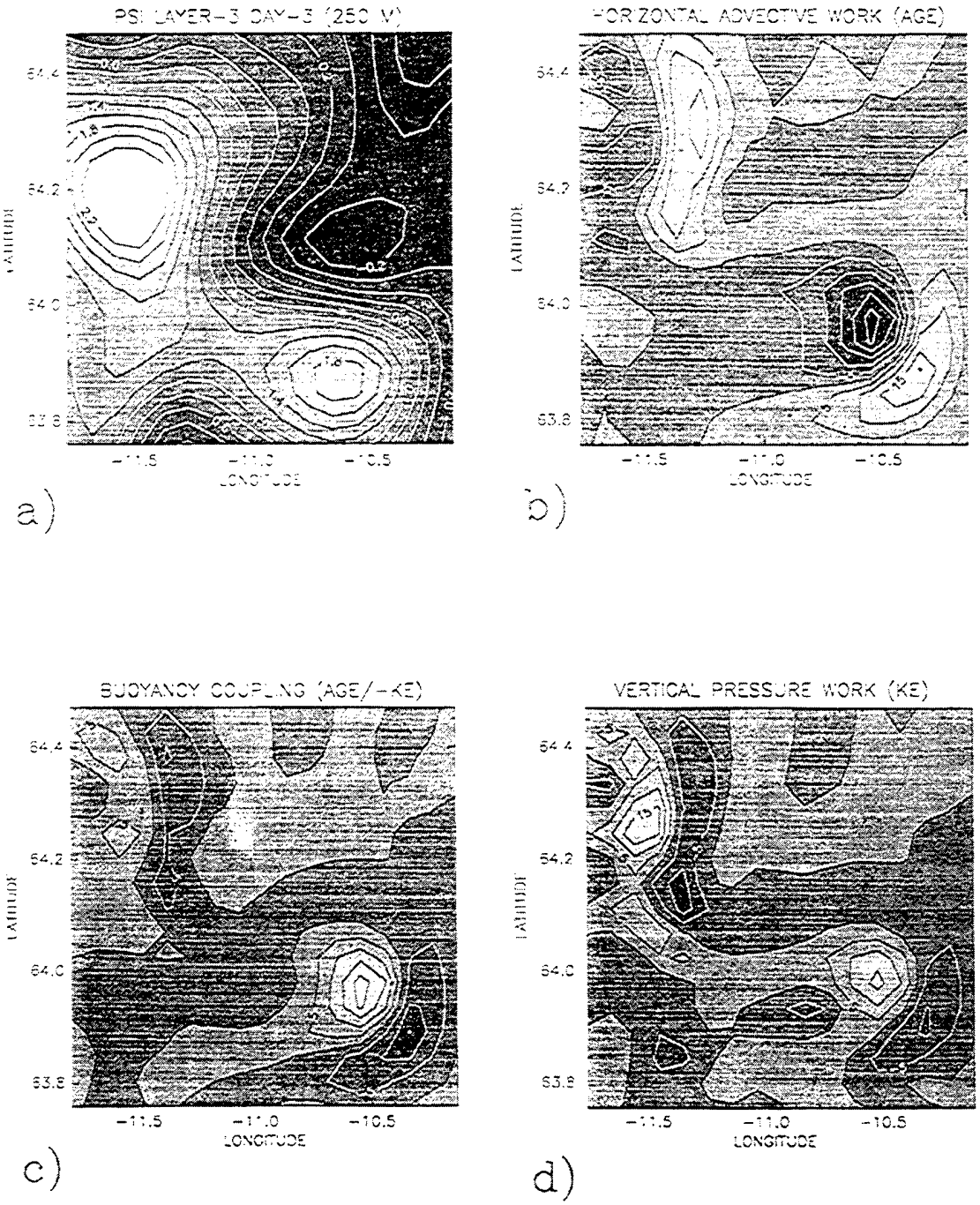

Figure 6. a) Forecast stream function at 250 m depth (QG model layer 3) for August 23, 1993, (forecast day 3). Contour interval is 0.25 nondimensional units. To redimensionalize to m^2/s, multiply plotted values by 4500. Spatial maps for the same day and layer of b) the horizontal AGE advective working rate c) the buoyancy working rate (oppositely signed in the AGE and KE equations) and d) the KE vertical pressure working rate. Contour interval is 5.0 nondimensional units. Unshaded areas lie between 0 and 5, lightest shading lies between 0 and -5.

helps to explain why the QG model (with a flat bottom) was able to adequately represent the explosive cold tongue and hammerhead intrusions in spite of the presences of very steep topography in the vicinity. A comparable energetics analysis of PE model forecasts, which can handle the steep bathymetry in this region, will provide more conclusive details of the physics. especially if forecast skill can be demonstrated beyond the 3–to–4 day range of the QG case.

6.3 Forecast Skill

Skill measures introduced in Section 5 are Pattern Correlation Coefficient (PCC) and Normalized Root Mean Squared Error (NRMSE). A positive PCC difference (or a negative NRMSE change) indicates higher skill for the forecast. Due to the existence of the front, correlations remain high even for persistence forecasts (e.g., typical values of the PCC exceed 0.6 for forecasts by persistence of day 0). It should be noted that even a slight improvement in PCC for a forecast can explain a fair percentage of additional pattern variance of the field. For example, if a forecast field has PCC = 0.85, representing an increase of 0.10 over a persistence forecast PCC = 0.75, 16 percent additional variance of the pattern of the field has been predicted, which is useful.

An oceanic data set adequate for quantitative skill assessment is provided by the August 1993 IFF experiment. The hydrographic data set consists of a complete initial survey (spanning 3 days), an updating assimilation zig-zag survey (over 2 days) and a complete validation survey (7 days later than the initial). The HOPS was invoked in several different forecast scenarios during that cruise, and significant quantitative skill scores have been obtained for both the PE model (Robinson *et al.*, 1995) and the QG model (Miller *et al.*, 1995b). A similar forecast by the PE model, which assimilated both the initial and the zig-zag surveys, successfully forecast middle and lower water column temperature better than persistence, increasing the PCC by more than 0.10 and reducing NRMSE by several tens of percent. In fact, the PE model captured the upper-water column structure of the observed hammerhead intrusion but forecast a hammerhead displaced slightly downstream of the observed, thus destroying the PCC. If that downstream shift (10 km) is accounted for by including a spatial lag in the PCC computation, the PE model PCC beats persistence by 0.14 and the RMSE is reduced by 0.15.

Skillful results were also obtained for upper-water column flows using the quasi-geostrophic forecast model (Miller et al., 1995b), although the QG model was unable to capture the sharp and narrow features of the hammerhead structure . However, the QG model was validated against dynamic height while the PE model was validated against temperature. A direct comparison between forecast PE and QG current or dynamic height fields has yet to be carried out. But since both the PE and (flat bottom) QG models exhibited upper-ocean forecast skill, we note that topographic influence was minimal during the 3 to 4 days of the simulations because the modeled instability apparently was trapped in the upper part of the water column. Only the PE model was able to forecast with fidelity the deep flows around the IFF.

7. THE STRAITS OF SICILY AND IONIAN SHELFBREAK REGIONS

The region of the Straits of Sicily, the Ionian shelf break and the western Ionian Sea has a complex geometry and topography (Fig. 7a). In the Straits, there are shallow coastal areas with depths less than 100 m. Off Tunisia, there is a broad gentle slope region extending eastward. There is a central narrow passageway which is most restricted at the western end. Deep trenches exist in the middle and other regions of the Straits with depths of 300–1500 m. Along the eastern coast of Sicily and extending southward, there is a narrow Ionian shelf break, which fans out and broadens off the coast of Libya.

In the Straits of Sicily, the fresh Atlantic inflow and the salty Levantine outflow constitute a two-current system of the general circulation of the eastern Mediterranean. The Levantine outflow is located at depth and the Atlantic inflow is in the upper ocean. The Atlantic inflow, which marks the beginning of the Atlantic-Ionian Stream (AIS), flows past Malta and turns northward where, we believe, it was first identified as a local feature over the shelf break, the Maltese Front (Johannessen *et al.*, 1971). Subsequently, the AIS flows off the shelf into the upper, western Ionian Sea, with an intense looping northward meander, which generally decreases in amplitude during the winter. Various analyses of data gathered in this region (Grancini and Michelato, 1987; Moretti *et al.*, 1993; Manzella *et al.*, 1990) have described the Atlantic inflow as having a filamented but predominantly two-jet structure spanning the upper 100 m, with an associated salinity minimum, flowing closest to Tunisia and along the coast. This region contains a number of significant processes and phenomena. In addition to the general circulation with its mesoscale variability, there are the wind-driven currents on the shelf from local and remote storms (including the Sicilian coastal current) and upwelling off Sicily. Tides, inertial, gravity, surface, and continental shelf waves occur. This region contains active water mass modification processes between the fresher and warmer Atlantic origin water mass and the saltier and colder Levantine water mass. The topographical complexity, multiplicity of scales, and circulation currents and structures make the Straits of Sicily, the Ionian shelf break and western Ionian Sea a most challenging region for the development of a regional ocean prediction system.

In November 1994, Harvard University and the SACLANT Undersea Research Centre carried out their first exploratory phase research cruise for the development of a forecast system for the Straits of Sicily and the Ionian shelf-break region. The observations (Fig. 7b) were gathered in two phases: (i) a survey with mesoscale resolution over a large region; and (ii) a survey with submesoscale resolution over a mesoscale region in the region of the Maltese Front segment of the AIS over the sharp Ionian shelf break, as shown in Figs. 7c and 7d. Here we present preliminary results of analyses and sample nowcasts and forecasts carried out at sea. A second forecast experiment is planned for October 1995.

7.1 Descriptive Oceanography

Analyses to date have identified interesting aspects of the complex circulation and water masses of the region. A water-mass model was constructed from the hydrographic data collected during the cruise. The CTD and XCTD profiles were analyzed for water-

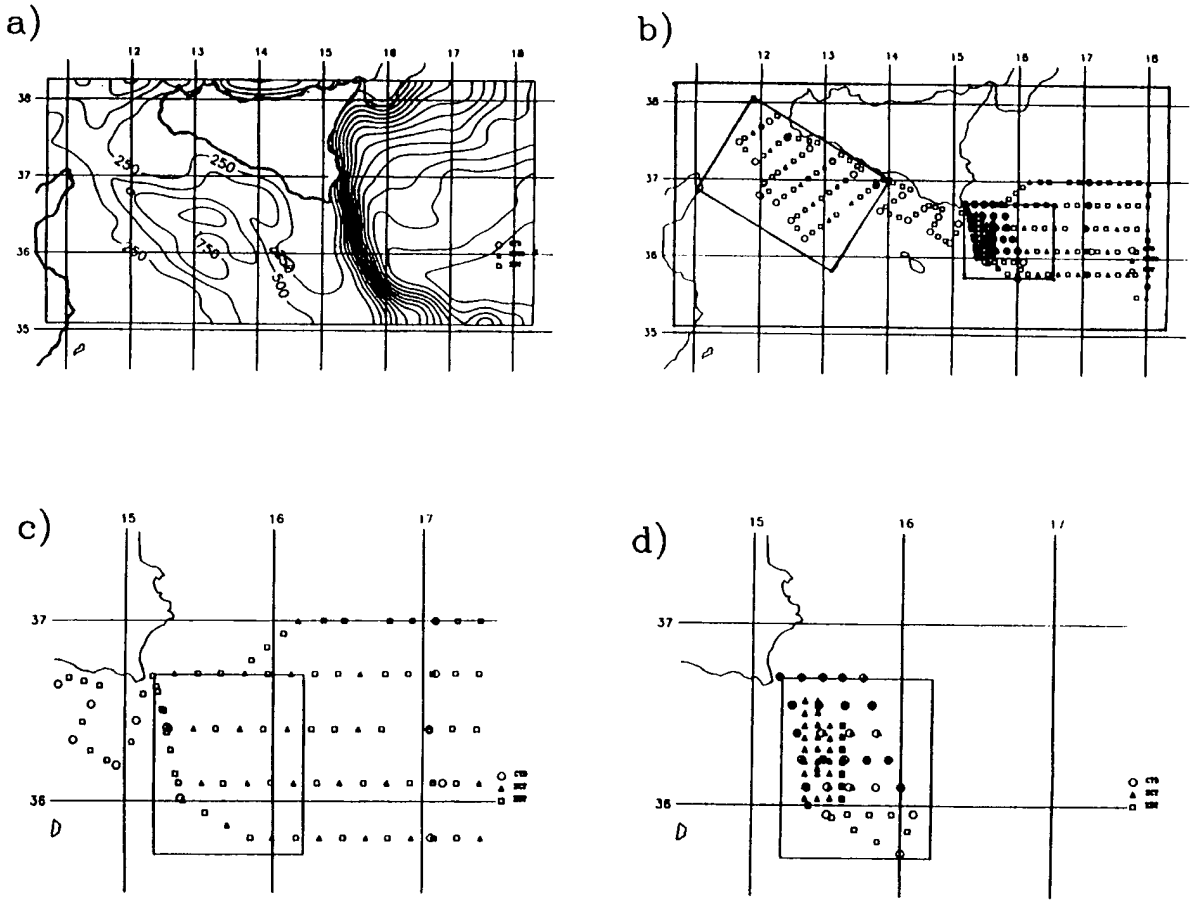

Figure 7. a) Bottom topography in Straits of Sicily and Ionian shelfbreak regions. Contour interval is 250 m. b) Hydrographic observations November 13–21, 1994. Indicated are the large and two nested modeling domains. c) and d) Observations in Ionian shelfbreak region at mesoscale and submesoscale resolution, respectively. For b), c) and d), CTDs are indicated by circles, XCTDs by triangles and XBTs by squares.

mass signatures. Seven water masses were identified among the measured temperatures and salinities, as sketched in Fig. 8. Moving from the Levantine water at the bottom towards the surface, one finds Transitional, Fresh, Mixed, (Modified) Atlantic, Upper, and Surface water masses. Not every water mass was found in the water column at every station. We comment briefly on the Atlantic water mass, as the kinematics and dynamics of the AIS were of special interest. It was found that the core of the Atlantic water mass was located below the mixed layer and spread throughout most of the survey region. In the center of the core, the salinities ranged from 37.4 to 38.0 PSU and temperatures from 16.5°C to 18.5°C. The thickness of the Atlantic layer ranged from 30 to 100 m, with center core depths 30 to 80 m below the surface. During the survey, the southwestern corner of the shelf break always contained a core of Atlantic water below the mixed layer. The rest of the shelf-break region exhibited variability in its upper layer Atlantic water content distribution. Research in progress includes horizontal mapping of the indices which characterize the depths of central and intermediate temperatures and salinities of the seven water masses (Fig. 8).

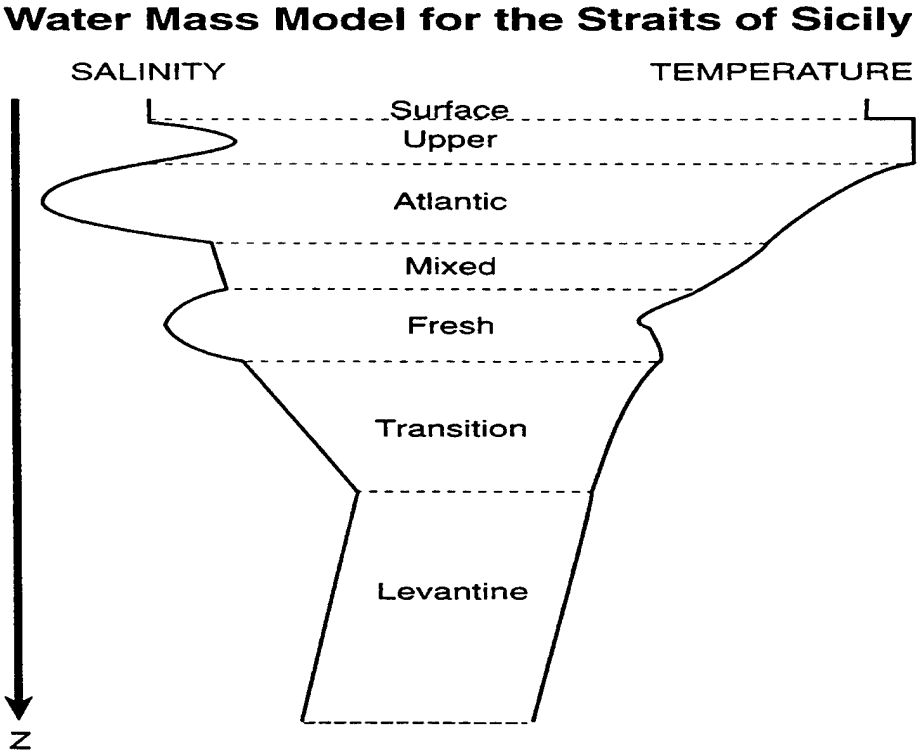

Figure 8. Water mass model for observations collected in Sicily Straits region in November 1994.

Figures 9a and 9b depict the temperature at 100 m on 16 and 19 November in the Ionian shelf-break region. These analyses reveal the rapid event-scale or submesoscale evolution which occur in the region of the shelf break. Clearly illustrated is the movement of mesoscale eddies just below the Maltese Front region of the AIS and lateral

shifts of 10–15 km in the frontal position over the brief interval of three days. This rapid evolution causes the accuracy of forecasts for small subregional domains to be highly dependent on boundary conditions.

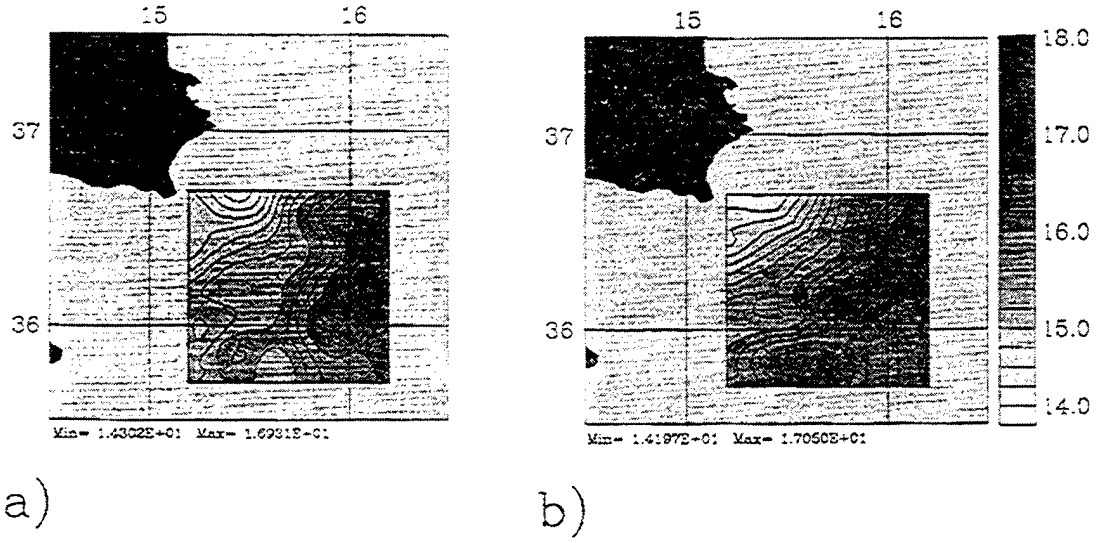

Figures 9a and 9b. Objectively analyzed temperature at 100 m using the data from November 15–17 and November 18–21, respectively.

7.2 Nowcasts and Forecasts

The region has complex topography and a variety of phenomena which makes forecasting challenging. As a result of this, a nesting strategy is adopted for the nowcasting/forecasting of this region. The real-time modeling domains were selected to be congruent with the sampling strategy. There is a large domain which covers all observational areas and two small domains which encompass the Straits of Sicily and Ionian observations (illustrated in Fig. 7b). The large domain has a 7.5 km resolution, whereas the small domains are resolved at 5 km. Each domain is modeled with 14 terrain-following vertical levels. The small Ionian domain is a very difficult one, as it is located in an area of steep and tall topography with a slope of about 12%.

The large domain contains areas which are well sampled (as indicated by the station symbols) and other areas in which no data was collected (south-west and north-east corners). For this experiment, the ship was restricted to sampling only in Italian waters. In the data-poor areas, climatology, historical synoptic data, and feature models are used in combination (melded) to provide initialization data. The large domain is initialized and forced with the melded feature model and climatology and the observations from multiple data streams are assimilated using the sequential updating

approach. Initial and boundary conditions are then extracted for the small domains from the large domain. The synoptic sampling was designed to yield adequate coverage for nowcasts and short-term forecasts in the small domains at the southwest and east of Sicily shown in Fig. 7b.

A sequence of real-time shipboard nowcasts and forecasts were carried out in the large and in the nested domains to test and tune model and sequential updating strategies. Figure 10a shows the temperature field at 50 m from a forecast for November 24 two days after the assimilation of all the cruise observations. One of the most notable features is the flow northward of the Maltese Front section of the AIS along the Ionian shelf-break region. Due to the lack of observations (Fig. 7b) south of Malta the synoptic structure of the AIS could not be definitively determined there.

The nowcasts and forecasts show that important mesoscale circulation elements can reasonably be reproduced. For instance, Fig. 10b shows the velocity and salinity field at 50 m of a forecast for November 14 in the nested Sicily Straits domain, obtained by sequential updating. The observations are assimilated in two stages; tracks 1-3 (western half) are assimilated at day 1 and tracks 4-6 (eastern half) are assimilated at day 2. The Atlantic Ionian current along the southern boundary of the domain and the structure of the coastal currents are well defined in the velocity and salinity fields. This figure also shows the fresher inflow of Atlantic water with salinities less than 37.5. Hindcasting research is now in progress to elucidate the forecasting potential of the November 1994 data set and to input to the design of our October 1995 cruise.

8. THE EASTERN MEDITERRANEAN

In early 1995, a multi-ship, multi-national experiment was conducted by the POEM-BC (Physical Oceanography of the Eastern Mediterranean with Biology and Chemistry) group in the Eastern Mediterranean to study the preconditioning, formation and spreading of Levantine Intermediate Water (LIW). Real-time regional forecasting, both shipboard and laboratory, was an integral component of the experiment, providing guidance for real-time design and modifications of the experiment as it occurred. Here we report our real-time nowcasting and forecasting during the first cruise of this experiment on board the *F/S Meteor* (January 10 to February 3) (Robinson *et al.*, 1995b). This initial survey was designed to determine the general circulation pattern and identify synoptic features during the preconditioning stage of the LIW formation, in conjunction with a transient-tracer and deep water experiment (Roether *et al.*, 1995). In general, this experiment can also be considered as contributing to the development of a basin-scale Eastern Mediterranean regional forecast system in both the exploratory (identification of regional scales, phenomena, processes and interactions) and dynamical phases (determination of synoptic flow structures, regional synoptical dynamical events, evolutions and interactions. As significant progress via other POEM work in the region had previously been made in the exploratory phase, this experiment should contribute significantly to the understanding of the dynamics of the region.

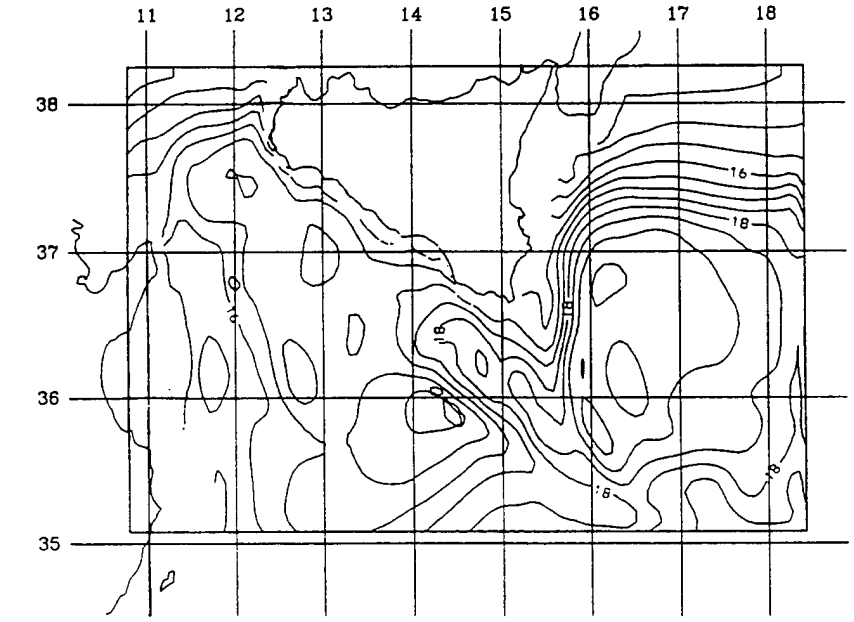

a)

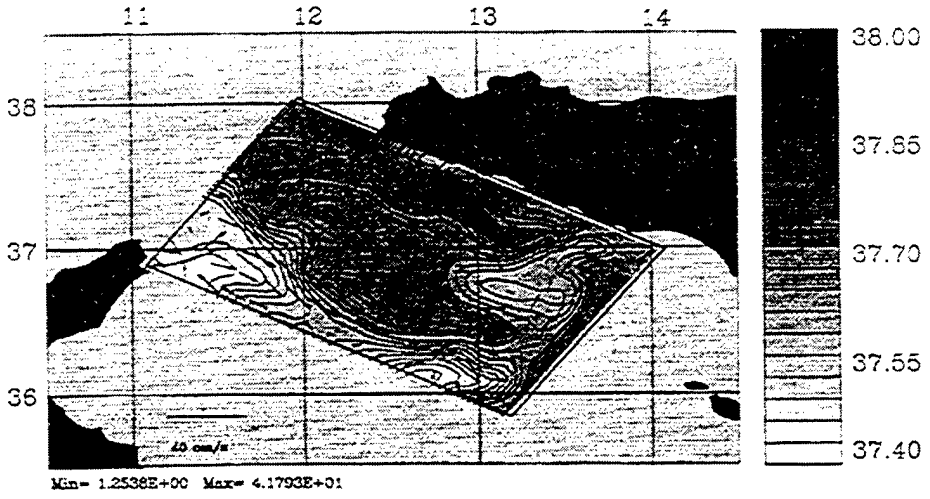

b)

Figure 10. A four-day forecast in the Sicily Straits domain. The observations are assimilated in two stages; tracks 1–3 (western half) are assimilated at day 1 and tracks 4–6 (eastern half) are assimilated at day 2. Salinity at 50 m is mapped with overlying velocity vectors. b) Two-day forecast temperature at 50 m in large modeling domain after assimilation of all observations.

Figure 11a shows the positions of the *F/S Meteor* data stations. Nearly 600 observations were made with CTDs (circles) and XBTs (squares). Along-track distance between XBTs was nominally 15 km in the Ionian basin (approx. 10–23° East) and 10 km in the Aegean Sea and Levantine basins (approx. 23-34° East). Sections along the entrances to the Adriatic and Aegean were sampled at 5 km resolution. CTD station locations were based on the needs of the tracer circulation study, hydrographic analysis and intercalibration stations for subsequent cruises. In order to maximize the use of the XBT data, a technique was used to combine the XBT temperature observations with the CTD salinity data. This technique involved identifying the individual CTD which best represented the temperature profile of the XBT and adding the CTD salinity to the XBT (with appropriate density constraints).

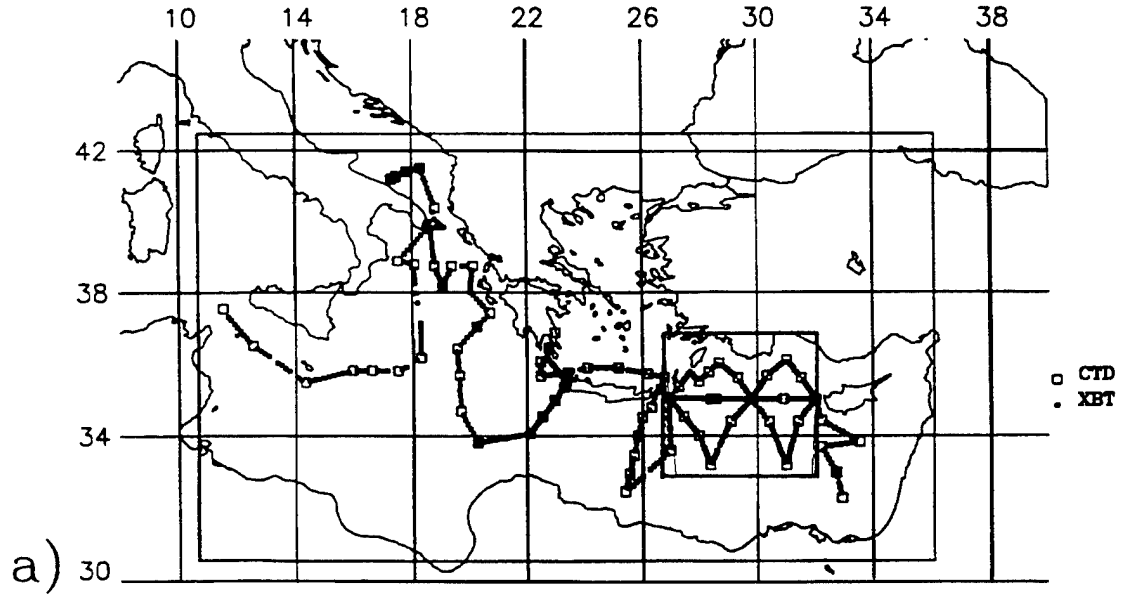

Figure 11a. Eastern Mediterranean CTD (squares) and XBT (dots) data collected during *F/S Meteor* cruise M31/1. Indicated are full Eastern Mediterranean and Levantine region modeling domains.

The modeling objectives for this cruise were to sea-test, in real-time, novel methods of nowcasting, forecasting and simulating real ocean multiscale synoptic fields involving: i) nested regions of high resolution within a full basin synoptic estimate; and, ii) the fusion of dynamics with various data types via multiple data streams, including historical synoptic realizations, climatologies and direct data streams acquired at sea. More specifically, the intent was to establish a synoptic circulation over the entire Eastern Mediterranean basin (the large box in Figure 11a), with an emphasis on the northwestern Levantine basin (the small box shown in Fig. 11a), where the LIW is thought to form.

The approach was to establish a background circulation which contained the major circulation elements in the basin and which could smoothly incorporate the ship

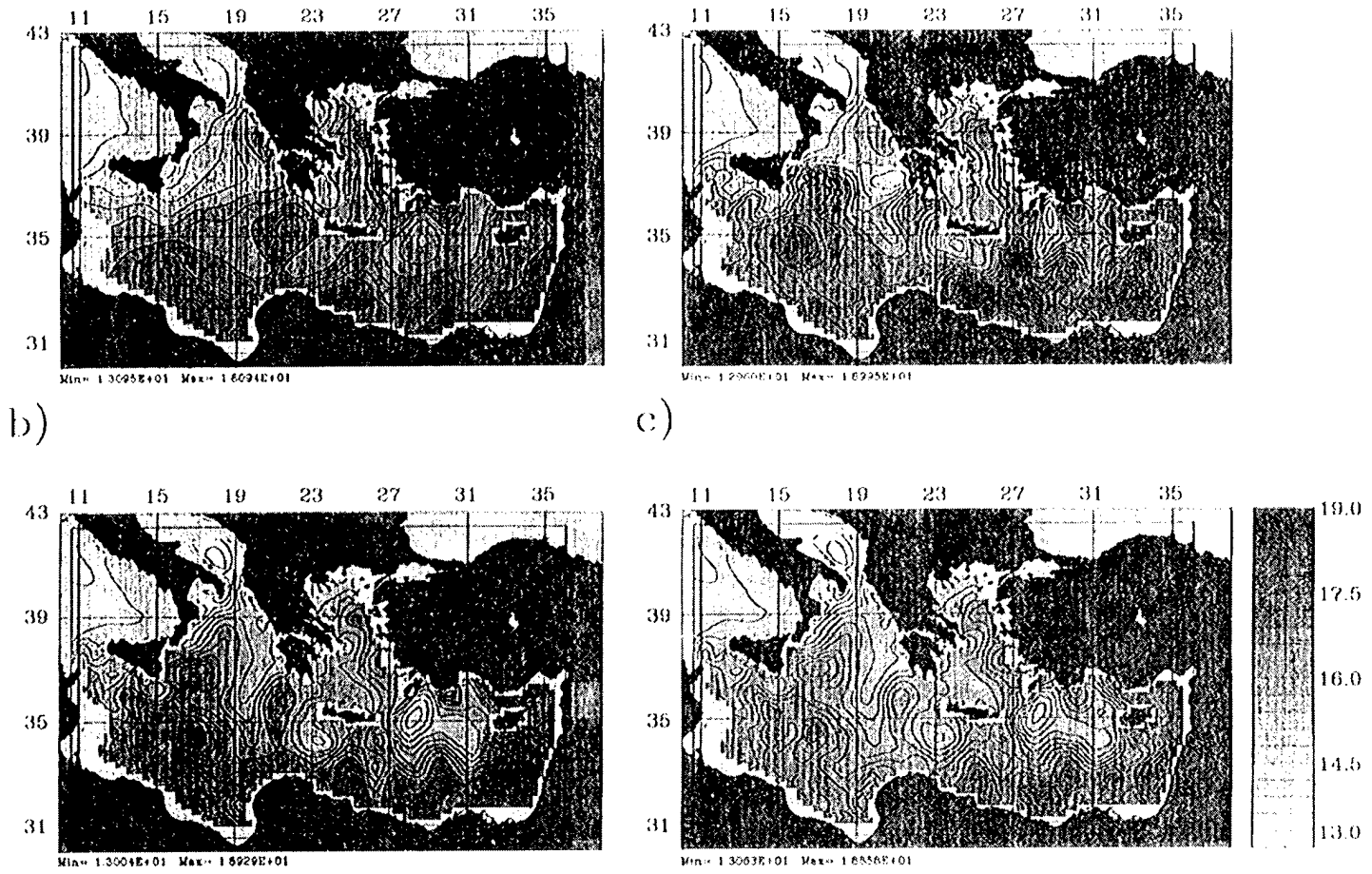

Figures 11b-d. Temperature at 125 m for: b) primitive equation model forecast initialization (day 0) from climatological data; c) forecast day 1, after the assimilation of two historical synoptic data sets; d) forecast day 11, after the assimilation of all but one day of ***F/S Meteor*** data; e) forecast day 12, after the complete assimilation of ***F/S Meteor*** data.

gathered observations. The process used to construct the model initialization fields is as follows. Selected elements of the regional, historical, synoptical, statistical data base (Section 3) were assembled. The Primitive Equation model was initialized with the Mediterranean Oceanic Data Base (MODB) (Brasseur *et al.*, 1995) winter climatology (Figure 11b). This provided a reasonable state for the time of year, but with smooth, broad features. Figure 11b shows the presence of the flow into the Eastern Mediterranean through the Straits of Sicily, the Pelops Gyre to the west of Crete, the Rhodes Gyre in the northwest Levantine, the Mid-Mediterranean Jet in the central Levantine and the general sense of the circulation in the Levantine. The model, forced with climatological wind stresses, was allowed to adjust, and then historical synoptic data was assimilated (Figure 11c). This data set included the November 1994 AIS data (Sicily Straits and Ionian basin east of Sicily; Section 7) and the December 1991 NAVO AXBT (complete Eastern Mediterranean; Horton *et al.*, 1994) data. The inclusion of this synoptic data introduces realistically structured conditions, tightens the fronts and reduces the size of eddies. There is no assumption that this synoptic data represents the oceanic structures of the period immediately prior to the present cruise. Rather, the introduction of this data creates a "typical" synoptic situation for this time of year. At this time, the circulation closely resembles the complex, linked, basin-scale circulation pattern (Fig. 12) which has been discovered by POEM research (Robinson and Golnaraghi, 1993).

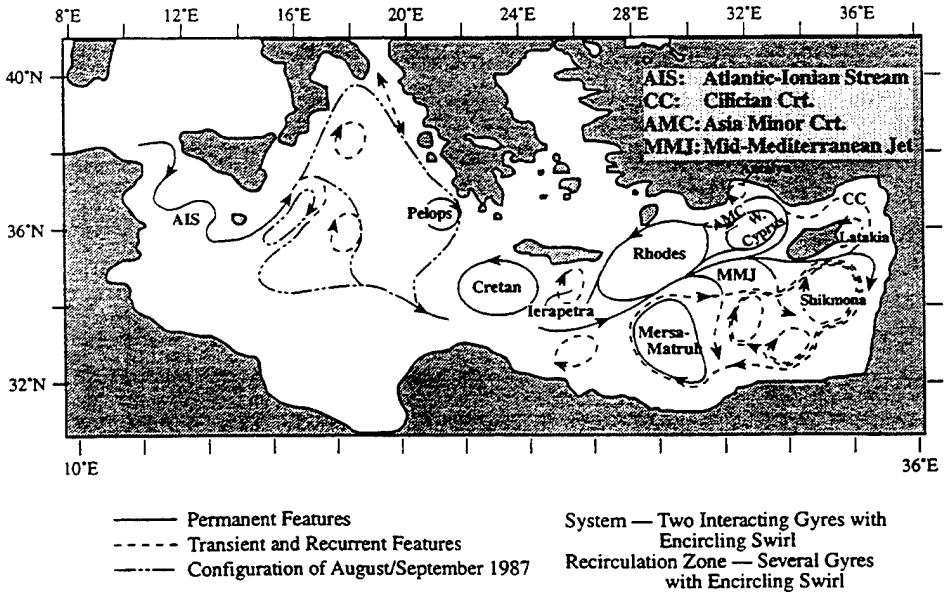

Figure 12. Schematic of Eastern Mediterranean circulation (after Robinson and Golnaraghi, 1993). Reprinted by the kind permission of Pergamon Press, Ltd.

The model is now in a state suitable for assimilating the 1995 *Meteor* data as it comes in. Figure 11d shows the model 11 days later, when almost all of the *F/S Meteor* data has been assimilated (only the final southeast leg is absent). Comparing with Figure 11c, we see that, along the ship's track, the synoptic features are corrected to their January 1995 locations. Features in the Ionian are adjusted and shifted, most notably in the western Ionian. The warm eddy at 37°N, 17°E is more clearly defined, as is the Pelops Gyre. Warm temperatures advance farther to the north and there is greater distinction between the waters of the central Ionian and coastal waters along the east coast of Italy. In the Levantine, however, the *Meteor* data indicates significant changes from the historical synoptic data. The Rhodes Gyre is considerably expanded and its borders well indicated. There is a strong temperature gradient from the eastern Aegean to the Rhodes Gyre. Figure 11e shows the final assimilation of the remainder of the *Meteor* data set (13 model days). The newest data is from the region south of Cyprus, towards Egypt (see Fig. 11a). While the west-east temperature gradient has been weakened somewhat, it remains intact and in place. This is an indication that the combination of climatology and historical synoptic data located reasonable features in reasonable places and that the *Meteor* data, in this small area, is providing only minor corrections to the initial and forecasted conditions.

The nested northwestern Levantine modeling domain, indicated in Fig. 11a, was initialized at day 11 from the field depicted in Figure 11d, providing a first guess to the circulation in the domain. Figures 13a and 13b show a two day forecast of temperature and density anomaly for this region. The cold core of the Rhodes Gyre is clearly defined. Analysis of the data and modeling results were sent from the ship to shore-based facilities in order to guide the design of subsequent cruises. Data gathered in the subsequent POEM LIW experiment cruises were essentially contained in this northwestern Levantine domain. The modeling research in progress involves nested domains, including the entire Eastern Mediterranean, the north-western Levantine and additional nested domains with mesoscale and submesoscale resolution using two way nesting.

9. DISCUSSION AND CONCLUSIONS

Modern research has revealed the synoptic states of the deep ocean and coastal seas to be a complex mix of interactive scales and circulation structures and variabilities. Thus the ocean prediction problem is complex and data requirements indicate that data assimilation is essential to the feasibility of nowcasting and forecasting. Unlike the atmospheric weather forecasting, ocean forecasting requires a regional approach, both from practical operational considerations and for the attainment of the accurate detailed realistic field estimates required for scientific research.

Regional ocean prediction system development involves three phases: exploratory, dynamical and predictive. General validation, regional calibration and qualitative verification are essential. The final system should be accurate and efficient with minimal observational resources, but such systems can only be achieved through forecast experimental oversampling. The approach taken with the Harvard Ocean Prediction System

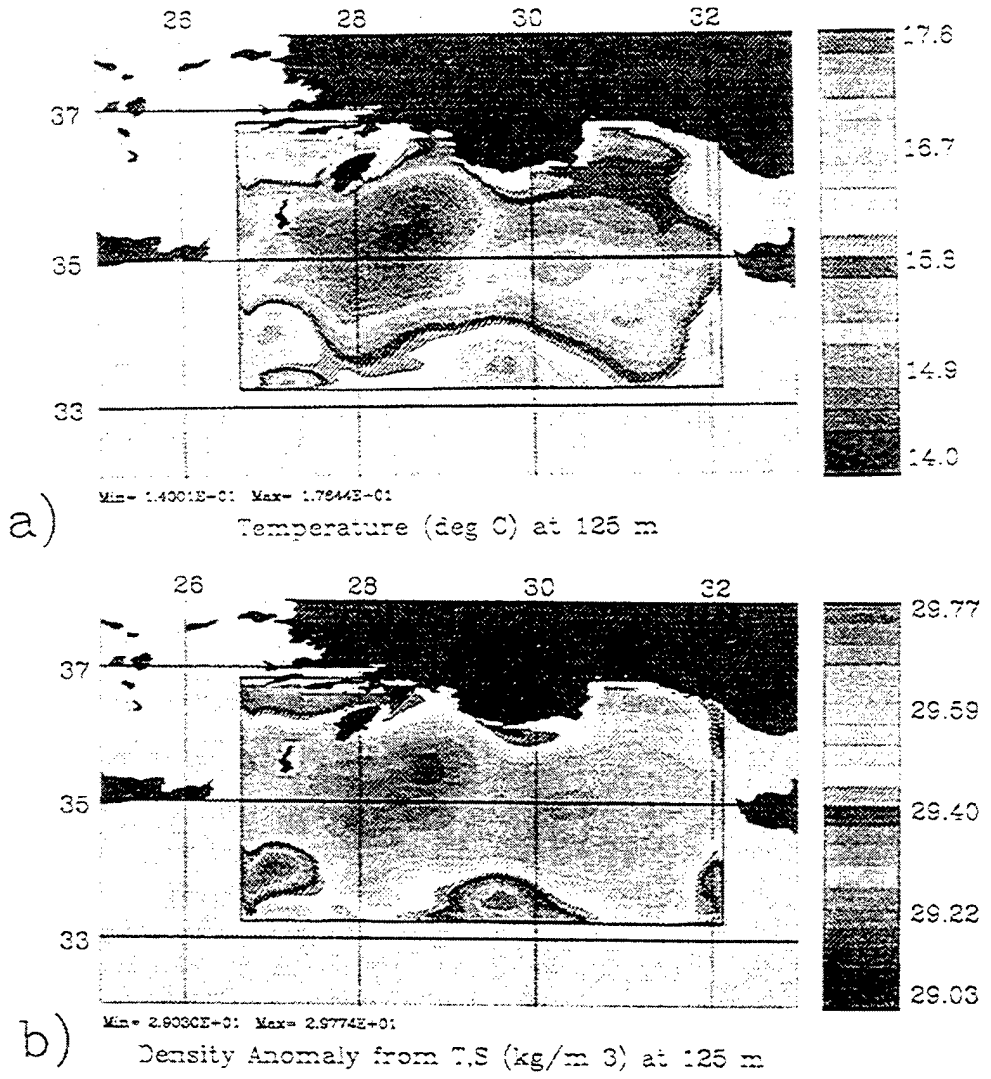

Figure 13. a) Levantine modeling domain day-2 forecast temperature at 125 m. b) As in a) but density anomaly.

(HOPS) involves initialization and assimilation of synoptic states constructed via the melding of multiple data streams, composed of real-time data streams, feature models, historical synoptic states, etc.. The synoptic accuracy of such states depends upon regional variabilities and the quantity of real-time data available, but, in any case, a reasonable and regionally typical evolving set of synoptic realizations is attained.

Recent real-time work at sea with HOPS has been reviewed and reported in the Iceland-Faeroe Frontal region, the Sicily Straits and the Eastern Mediterranean basin. The concept of an optimal synoptic representation of a region via the method of sequential updating has been proposed. This concept requires testing and development via the obtainment of truly regional synoptic time series which will require some mix of multiple platforms and remote sensing. Research is also required for an improved assimilation scheme for sequential updating to replace our simple optimal interpolation. Substantial further research is also required in the areas of nesting and multiple-data-stream melding, which have been initiated during these recent real-time shipboard nowcasts and forecasts.

Ocean prediction, in general, and regional prediction, in particular, are presently rapidly evolving. Indications are that ocean science and marine technology can benefit substantially in the near future by the practical availability, on a substantial basis, of realistic field estimates for operations, research and management purposes.

10. ACKNOWLEDGEMENTS

We thank Dr. Charles Horton (Naval Oceanographic Office) for providing the Eastern Mediterranean AXBT data. The CTD data set in the Eastern Mediterranean was obtained by Dr. Beniamino Manca (OGS - Trieste, Italy) aboard the ***F/S Meteor***, as part of the POEM LIW experiment. We thank Prof. Wolfgang Roether for immediate access to this data, which facilitated the generation of nowcasts at sea; and his useful discussions with one of us (ARR). Special thanks to the Deutsche Forschungsgemeinschaft, Bonn-Bad Godesberg, Germany for making possible our participation in the M31/1 cruise on the ***F/S Meteor***. The assistance of Dr. Pierre-Marie Poulain and Mr. Quinn Sloan at sea aboard the ***R/V Alliance*** in the Iceland-Faeroe Front and Straits of Sicily is acknowledged with thanks. On these cruises, the expertise and performance of both the technical staff of SACLANT Centre and the Captain and the crew of the ***R/V Alliance*** were essential for success. We thank Ms. Marsha Glass for the efficient logistics during our cruises. We acknowledge the Office of Naval Research for support of this research and enabling the acquisition of the XBT probes required for the mesoscale sampling conducted on the ***F/S Meteor*** (grants N00014–91–I–0577, N00014–90–J–1612, N00014–94–1–G915 and N00014–91–J–1521 (Ocean Educators Award)). Support from the National Science Foundation, grant OCE-9403467, is gratefully acknowledged.

REFERENCES

Arango, H.G., A.R. Robinson, M. Golnaraghi, N.Q. Sloan, P.-M. Poulain, A. Miller, and A. Warn-Varnas (1993) Real time nowcasting and forecasting, SACLANT Undersea Research Centre R/V Alliance GIN92 cruise, 13–29 October 1992: at sea real-time forecasts using primitive equation, quasigeostrophic, coupled surface boundary layer, and parabolic equation acoustic models. ***Technical Report***, Harvard University, Cambridge, MA.

Bennett, A.F. (1992) ***Inverse Methods in Physical Oceanography.*** Cambridge University Press, 346 pp.

Brasseur, P., J.M. Beckers, J.M. Brankart and R. Schoenauen (1995) Seasonal Temperature and Salinity Fields in the Mediterranean Sea: Climatological Analyses of an Historical Data Set (submitted).

Clancy, R.M. (1992) Operational modeling: ocean modeling at the Fleet Numerical Oceanography Center. ***Oceanography*** **5**(1), 31–35.

Denbo, D.W. and A.R. Robinson (1988a) Harvard gapcasts; a progress report: regional forecasting, processes and methodology in the Iceland-Faeroe Island gap. Part I: Data forecast and hindcast experiments. ***Reports in Meteorology and Oceanography: Harvard Open Ocean Model Reports,*** **32**, Harvard University, Cambridge, MA.

Denbo, D.W. and A.R. Robinson (1988b) Harvard gapcasts; a progress report: regional forecasting, processes and methodology in the Iceland-Faeroe Island Gap. Part II: GFD and process experiments. ***Reports in Meteorology and Oceanography: Harvard Open Ocean Model Reports,*** **33**, Harvard University, Cambridge, MA.

Dickey, T.D. (1993) Technology and Related Developments for Interdisciplinary Global Studies. ***Sea Technology***, 47–53.

Durham, D.L. and J.K. Lewis (1992) Introduction: Oceanic and atmospheric nowcasting and forecasting. ***Marine Technology Society Journal*** **29**(2), 3–4.

Gangopadhyay, A., A.R. Robinson and H.G. Arango (1995) Circulation and Dynamics of the Western North Atlantic, I: Multiscale Feature Models (submitted, ***Journal of Atmospheric and Oceanic Technology***).

Gangopadhyay, A., and A.R. Robinson (1995) Circulation and Dynamics of the Western North Atlantic, III: Forecasting the Meanders and Rings (submitted, ***Journal of Atmospheric and Oceanic Technology***).

Golnaraghi, M. (1993a) Circulation and dynamics of the Eastern Mediterranean Sea, Ph.D. thesis, Harvard University, 1993; ***Reports in Meteorology and Oceanography,*** **49**, Harvard University, Cambridge, MA.

Golnaraghi, M. (1993b) Dynamical studies of the Mersa Matruh gyre: intense meander and ring formation events. ***Deep-Sea Research*** **40**(6), 1247–1267.

Grancini, G. and A. Michelato (1987) Current structure and variability in the Straits of Sicily and adjacent areas. ***Annales Geophysicae*** **5B**(1), 75–88.

Horton, C., J. Kerling, G. Athey, J. Schmitz, and M. Clifford (1994) Airborne expendable bathythermograph survey of the Eastern Mediterranean. ***Journal of Geophysical Research*** **99** C5, 9891–9905.

Johannessen, O.M., F. De Strobel, and C. Gehin (1971) Observations of an oceanic frontal system east of Malta 1971 (May Frost). ***SACLANTCEN TM-169.*** La Spezia, Italy,

NATO SACLANT Undersea Research Centre.

Lai, C.A., W. Qian, and S.M. Glenn (1994) Data assimilation and model evaluation data sets. ***Bulletin of the American Meteorological Society*75**, 793–810.

Lozano, C.J., A.R. Robinson, H.G. Arango, A. Gangopadhyay, N.Q. Sloan, P.J. Haley, L.A. Anderson, and W.G. Leslie (1995) An Interdisciplinary Ocean Prediction System: Assimilation Strategies and Structured Data Models. In ***Modern Approaches to Data Assimilation in Ocean Modeling***, P. Malanotte-Rizzoli, editor.

Lynch, D.R. (ed.) (1995) Quantitative Skill Assessment for Coastal Ocean Models. Coastal and Estuarine Studies, Volume 47, American Geophysical Union.

Malanotte-Rizzoli, P. and E. Tziperman (1995) The Oceanographic Data Assimilation Problem: Overview, Motivation and Purposes. In ***Modern Approaches to Data Assimilation on Ocean Modeling***, P. Malanotte-Rizzoli, editor.

Manzella, G.M.R., T.S. Hopkins, P.J. Minnett, and E. Nacini (1990) Atlantic Water in the Straits of Sicily. ***Journal of Geophysical Research* 95**, 1569–1575.

Miller, A.J., H.G. Arango, A.R. Robinson, W.G. Leslie, P.-M. Poulain and A. Warn-Varnas (1995a) Quasigeostrophic forecasting and physical processes of Iceland-Faeroes Frontal variability. ***Journal of Physical Oceanography* 25**, 1273–1295.

Miller, A.J., P.-M. Poulain, A.R. Robinson, H.G. Arango, W.G. Leslie, and A. Warn-Varnas (1995b) Quantitative Skill of Quasigeostrophic Forecasts of a Baroclinically Unstable Iceland-Faeroe Front. ***Journal of Geophysical Research* 100**, C6, 10,833–10,849.

Mooers, C.N.K., A.R. Robinson and J.D. Thompson (1986) ***Ocean Prediction Workshop*** 1986 ***A status and prospectus report on the scientific basis and the Navy's needs.*** Proceedings of the Ocean Prediction Workshop. Institute for Naval Oceanography, NSTL, MS.

Moretti, M., E. Sansone, G. Spezie, and A. De Maio (1993) Results of investigations in the Sicily Channel (1986-1990). ***Deep-Sea Research II* 40**(6), 1181–1192.

Peggion, G. (1991) Diagnostic calculations for the reconstruction of environmental and acoustic conditions in the Iceland-Faeroe Ridge region during June 1989, ***SACLANTCEN SR-178.*** La Spezia, Italy, NATO SACLANT Undersea Research Centre, 65 pp.

Peloquin, R.A. (1992) The Navy ocean modeling and prediction program. ***Oceanography.*** **5**(1), 4–8.

Pinardi, N. and A.R. Robinson (1986) Quasigeostrophic energetics of open ocean regions. ***Dynamics of Atmospheres and Oceans* 10**(3), 185–221.

Pinardi, N. and A.R. Robinson (1987) Dynamics of deep thermocline jets in the POLYMODE region. ***Journal of Physical Oceanography*, 17**, 1163–1188.

Robinson, A.R. (ed.) (1983) ***Eddies in Marine Science***, edited and with an introduction by A.R. Robinson, Springer-Verlag, 609 pp.

Robinson, A.R. (1992) Shipboard prediction with a regional forecast model. ***The Oceanography Society Magazine*** **5**(1), 42–48.

Robinson, A.R. (1995) Physical processes, field estimation and interdisciplinary ocean modeling. ***Earth-Science Reviews*** (in press). Also available as ***Harvard Open Ocean Reports* 51**, Harvard University, Cambridge MA.

Robinson, A.R., J.A. Carton, N. Pinardi and C.N.K. Mooers (1986) Dynamical forecasting

and dynamical interpolation: an experiment in the California Current. ***Journal of Physical Oceanography*, 16**, 1561–1579.

Robinson, A.R., M.A. Spall, and N. Pinardi (1988) Gulf Stream simulations and the dynamics of ring and meander processes. ***Journal of Physical Oceanography*** **18**(12), 1811–1853.

Robinson, A.R., H.G. Arango, W.G. Leslie, P.F. Lermusiaux and P.-M. Poulain, A. Miller, A. Warn-Varnas, G. Baldasserini-Battistelli, M. Zahorodny, and P. Zanasca (1994) Real-time nowcasting and forecasting, R/V Alliance GIN93 cruise, 11–26 August 1993: operational forecasts and simulation experiments at sea. ***Harvard Open Ocean Reports*** **50**, Harvard University, Cambridge, MA.

Robinson, A.R. and A. Gangopadhyay (1995) Circulation and Dynamics of the Western North Atlantic, II: Dynamics of Meanders and Rings (submitted, ***Journal of Atmospheric and Oceanic Technology***).

Robinson, A.R. and M. Golnaraghi (1993) Circulation and Dynamics of the Eastern Mediterranean Sea; quasisynoptic data-driven simulations. ***Deep-Sea Research*** **40**(6), 1207–1246.

Robinson, A.R., H.G. Arango, A.J. Miller, A. Warn-Varnas, P.-M. Poulain, and W.G. Leslie (1995a) Real-Time Operational Forecasting on Shipboard of the Iceland-Faeroe Frontal Variability. ***Bulletin of the American Meteorological Society*** (in press).

Robinson, A.R., H.G. Arango, W.G. Leslie, H.M. Hassan, A.M. Mahar, and M. Candouna (1995b) XBT Data, Hydrographic Analyses, Nowcasts and Forecasts: F/S Meteor 31/1 (POEM-BC LIW 95) Cruise Report. ***Harvard Open Ocean Reports***, Harvard University, Cambridge, MA

Roether, W., B. Manca, B. Klein, D. Bregant, and D. Georgopoulos (1995) Eastern Mediterranean deep waters found in an entirely new state (submitted).

Spall, M.A. (1989) Regional primitive equation modeling and analysis of the POLYMODE data set. ***Dynamics of Atmospheres and Oceans*** **14**, 125–174.

Spall, M.A. and A.R. Robinson (1990) Regional primitive equation studies of the Gulf Stream meander and ring formation region. ***Journal of Physical Oceanography*** **20**(7), 985–1016.

Willems, R.C., S.M. Glenn, M.F. Crowley, P. Malanotte-Rizzoli, R.E. Young, T. Ezer, G.L. Mellor, H.G. Arango, A.R. Robinson, and C.-C. Lai (1994) Experiment evaluates ocean models and data assimilation in the Gulf Stream. ***EOS*** **75**(34).

Real-Time Operational Forecasting on Shipboard of the Iceland–Faeroe Frontal Variability

A. R. Robinson,* H. G. Arango,* A. J. Miller,+
A. Warn-Varnas,#,& P.-M. Poulain,# and W. G. Leslie*

ABSTRACT

Real-time operational shipboard forecasts of Iceland–Faeroe frontal variability were executed for the first time with a primitive equation model. High quality, intensive hydrographic surveys during August 1993 were used for initialization, updating, and validation of the forecasts. Vigorous and rapid synoptic events occurred over several-day timescales including a southeastward reorientation of the Iceland–Faeroe Front and the development of a strong, cold deep-sock meander. A qualitative and quantitative assessment of the skill of these forecasts shows they captured the essential features of both events. The anomaly pattern correlation coefficient and the rms error between forecast and observed fields are particularly impressive (and substantially superior to persistence) for the forecast of the cold meander.

1. Introduction

Oceanic synoptic–mesoscale variability is dynamically analogous to atmospheric synoptic-scale phenomena and represents the internal weather of the sea. Prediction of ocean mesoscale variability is interesting and important for both scientific and application purposes. Although rapid progress is occurring in ocean forecast research, oceanographers are still far behind meteorologists in their numerical weather prediction capabilities. We report here the successful results of real-time shipboard forecasting of vigorous mesoscale meandering and eddying of the frontal system between Iceland and the Faeroe Islands, called the Iceland–Faeroe Front (IFF).

The forecasts were performed onboard ship [the NATO (North Atlantic Treaty Organization) research vessel *Alliance*] and in real time during 15–24 August 1993. A primitive equation numerical model was used and data assimilation was carried out with an optimal interpolation scheme. The forecasts were of 7 days duration and were performed in an operational mode; that is, they were issued according to a regular and preset schedule. Data for model initialization, updating, and verification were gathered by the ship. Auxiliary forecasts were also carried out with a quasi-geostrophic model and a coupled surface boundary layer model driven by atmospheric fluxes. Using the forecasts by the primitive equation model as input, forecasts of time- and range-dependent acoustic propagation were executed with a parabolic equation acoustical model.

Oceanographers commonly refer to the energetic variability, which occurs on spatial scales characterized by the internal Rossby radius of deformation, as mesoscale variability (Robinson 1983), although the scientific analog is to the atmospheric synoptic scale. The internal radius in the ocean ranges from less than 10 km to several tens of kilometers and thus is two orders of magnitude or more smaller than the internal radius in the atmosphere. In the Iceland–Faeroe region the internal radius is only approximately 10 km. The small spatial scale of the variability makes research difficult and the development of forecasting a challenging task. Although realistic global- and ba-

*Division of Applied Sciences, Department of Earth and Planetary Sciences, Harvard University, Cambridge, Massachusetts.
+Scripps Institution of Oceanography, La Jolla, California.
#SACLANT Undersea Research Centre, La Spezia, Italy.
&Naval Research Laboratory, Stennis Space Center, Minnesota.
In final form 5 June 1995.
Corresponding author address: Prof. Allan R. Robinson, Division of Applied Sciences, Pierce Hall, Harvard University, Cambridge, MA 02138.

sin-scale ocean forecasts with mesoscale resolution are not yet feasible, regional forecasts are. Timescales of ocean mesoscale variability range from days to months. Because the variability is episodic and intermittent, an oceanic region is generally characterized by two timescales, one for the evolution and propagation of features and a second shorter one for the occurrence of energetic synoptic dynamical events. Such events—for example, the rapid nonlinear cresting of a meander or the snapping off of a ring eddy from a current—are generally localized and may be referred to in the spatial sense as submesoscale. Two timescales are known to characterize the Iceland–Faeroe frontal region where bursts of baroclinic instability cause rapid evolution (Miller et al. 1995a,b).

From a scientific viewpoint, nowcasting and forecasting oceanic mesoscale variability is important in order to efficiently use research resources in the intermittent ocean. Forecasting knowledge allows for the effective use of resources by "going to the right place at the right time." Nowcasts and forecasts are essential for the rapid assessment of a region for naval operations. Environmental factors associated with the water column, such as thermal gradients, can affect, for example, the distribution of free-floating mines or antisubmarine warfare tactics. Transport and distribution of nutrients and pollutants require forecasting in areas of coastal zone and fisheries management. General management and operational applications are discussed by Durham and Lewis (1992) and Peloquin (1992) in introductions to special issues of the *Marine Technology Society Journal* and *Oceanography,* respectively, which provide good reviews of the field. The real-time shipboard problem is introduced by Robinson (1992). Although mesoscale forecasting research is only about a decade old (Mooers et al. 1986), operational forecasts have been initiated for the Gulf Stream region (Clancy 1992). This is the region where a relatively good quality dataset (Lai et al. 1994) has also been assembled for forecast and simulation validation, and preliminary results are presented by Willems et al. (1994).

In this paper we describe, interpret, and evaluate the real-time primitive equation (PE) forecasts with optimal interpolation (OI) data assimilation made for the Iceland–Faeroe frontal system in August 1993. To our knowledge, it is the first time such forecasts have been made onboard ship and in an operational mode. Moreover, the forecast experiment was designed to acquire adequate data for PE model assimilation and verification. Unusually good weather allowed the ship to acquire the complete, accurate high-resolution dataset for these purposes. Several-day forecasts validate successfully both qualitatively and quantitatively, with the occurrence of two vigorous synoptical–dynamical events that were not present in initialization data. A rapid straightening and shifting of the frontal current was followed by the development of an intense deep-sock meander. The term "sock" describes the meander's general shape and has been in use since the early 1960s (Fuglister 1963).

In the following, we review the phenomenology of the IFF system, present the data and describe the synoptic variability observed, discuss forecast methodology, present and evaluate the forecasts, and discuss conclusions.

2. The Iceland–Faeroe frontal system

The IFF is located between Iceland and the Faeroe Islands in a region where the ocean bottom rises to within 400 m of the surface. The front forms the intersection of the warm saline North Atlantic water mass and the cold low-salinity Arctic water mass. Strong currents and sharp temperature gradients are found in this area. The classic picture of the temperature front in summer is shown in Fig. 1, from the 1958 International Geophysical Year surveys (Dietrich 1969).

From various studies, a composite picture of the current structures has emerged that shows a flow along the frontal area with inflow from the North Atlantic along the southeastern Icelandic shelf. Some inflow of Arctic-type water occurs along the northeastern Icelandic shelf and merges with the North Atlantic water inflow at the frontal location off Iceland (Peggion 1991). In the frontal region, a high degree of mesoscale dynamical activity exists. Frontal meanders and cold and warm eddies are present. Atmospheric cooling, mixing of the upper ocean, internal tides, and waves occur.

In the last few decades, a multitude of efforts for describing the thermal and current structures in the IFF have been conducted. These efforts began with the interpretations of the 1960 Overflow Expedition data by Hansen and Meincke (1979), who showed the existence of cold anomalies south of the IFF and warm ones just north of it. Hansen and Meincke proposed that the anomalies were caused by rapidly changing mesoscale eddies. This conjecture remained to be verified, as the 1960 Overflow Expedition surveys did not map the mesoscale field with sufficient resolution.

Studies of current meter data from the Monitoring the Overflow in the North Atlantic (MONA) project reveal that the timescale of subtidal fluctuations is on the order of a few days (Willebrand and Meincke 1980). The correlations between the velocity and temperature time series imply that there is conversion from mean potential energy to eddy kinetic, an expression of the baroclinic instability process.

Subsequent surveys and studies increased the documentation of the complicated eddy and frontal structures in the IFF (Smart 1984; Gould et al. 1987; Scott and McDowall 1990; Hopkins 1991; Niiler et al. 1992; Read and Pollard 1992; Perkins 1992; Allen et al. 1994; Miller et al. 1995a,b). The fine-resolution sections of these experiments were in the range of 4–7 km along tracks and 16–24 km between them. This enabled the quantification of the size and strength of the mesoscale and studies of the IFF dynamics. Denbo and Robinson (1988a,b) obtained a coarse mesoscale resolution time series of synoptic realizations of the IFF and initiated quasigeostrophic forecast experiments.

From the data, a picture of the eddy population in the IFF region is starting to emerge. Interpretation of the survey conducted by Gould et al. (1987) shows 7 cold eddies south of the IFF; Niiler et al. (1992) and Scott and Lane (1990) located 10 cold eddies of 30–50-km size and only 1 warm eddy north of the IFF. Allen et al. (1994) found a number of cold-core cyclonic eddies of 15–30 km and a few warm anticyclonic features. For the interpretation of the statistics of the data, Niiler et al. (1992) suggest that the dynamical situation for cold eddy formation is analogous to that of the Gulf Stream.

Recently, Miller et al. (1995a) have extended the synoptic description of the IFF evolution further by a direct model simulation of an observed instability. A typical rapid growth cold-tongue intrusion observed along the IFF, during a cruise in the fall of 1992, was diagnosed to be due to a baroclinic instability mechanism. It was shown that energy is drawn from the mean vertical shear at middepth and transferred to the mid- and upper-level kinetic energy. The effects of topography are minimized because the burst instability mechanism appeared to be surface intensified and occurred very rapidly in a submesoscale region.

3. Data and objective analysis maps

In August 1993, the Supreme Allied Commander, Atlantic (SACLANT) Undersea Research Center (SACLANTCEN) and Harvard University performed a joint hydrographic survey of the IFF for the purposes of real-time nowcasting and forecasting of IFF variabilities and studies of physical processes within the region (Poulain 1993; Robinson et al. 1994).

The general location of the experiment is shown in Fig. 2a, in which is outlined the observational and modeling domain, centered at 64.25°N, 10.75°W and 140 km in longitudinal extent and 190 km in latitudinal extent. This domain is enlarged in Fig. 2b, which shows the detailed underlying bottom topography that is input to the model. The experimental domain is essentially located on the top of the Iceland–Faeroe Ridge that descends into the Greenland–Iceland–Norway (GIN) Sea to the north and the North Atlantic to the south. Except for the northeast corner, the forecast domain is fairly flat in the south (about a 500-m depth) and uniformly sloped up to the west in the north. The model topography has been smoothed and conditioned (Lozano et al. 1994), which can limit a model's ability to capture certain small-scale dynam-

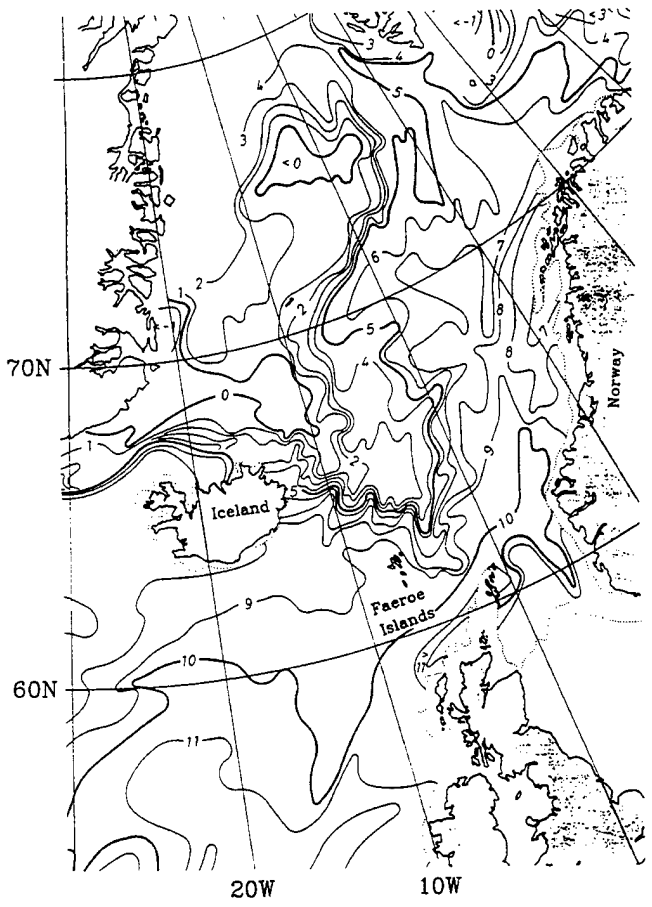

FIG. 1. Temperature at 100 m during the summer in the region of the Greenland–Iceland–Norway Sea. Contour interval is 1°C (from Dietrich 1969).

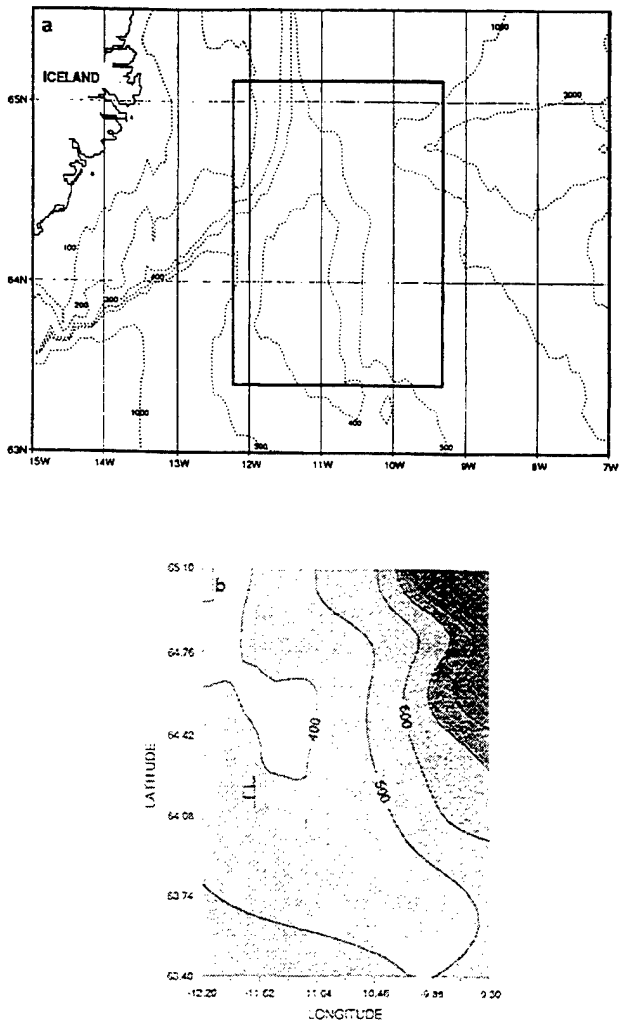

FIG. 2. (a) Map of the topography southeast of Iceland, showing the model domain (inner box). (b) Smoothed and conditioned topography used in the domain of the primitive equation model (Contour interval is 100 m).

ical events, such as density-driven overflows through narrow topographic gaps. Our model, on the other hand, feels the larger-scale dynamical effect of this topography as it affects the barotropic and baroclinic evolution of the unstable IFF current. Since the IFF current and its associated eddy field tends to be surface intensified, our smoothed rendition of the true topography will have a satisfactory dynamical effect on the anticipated mid- to upper water column burst instability events that are known to occur in this region and that result in the ambient eddy field. Furthermore, although our hydrographic sampling grid was not designed to properly resolve possible deep overflow events through narrow gaps, those thermohaline events are rare and are probably not directly coupled to the larger-scale IFF current variations that the model is fully capable of simulating.

The expendable bathythermograph (XBT), conductivity–temperature–depth (CTD), and expendable CTD (XCTD) data were grouped into three separate surveys (Figs. 3a–c), hereinafter referred to as the initialization, zigzag, and validation surveys. The subdomains on Figs. 3b,c are forecast evaluation domains to be described in section 6. Besides the hydrocasts, we deployed two sets of surface drifters (Poulain 1993) in the axis (18–19 August) of the IFF. One clear satellite image of SST in the survey area was also available for 22 August (Fig. 5).

To optimize the potential for quantitative forecast verification, the sampling locations and ship tracks of the initialization and validation surveys were identical. Since the ship entered the experimental domain from the east, the patterns were occupied from east to west. The zigzag survey was designed in real time to pinpoint forecast positions of the IFF during nighttime operations, while current meter moorings were being recovered during daylight. As the mooring data were not telemetered, it was not possible to use the data during the real-time forecasting. An analysis of the mooring data has been performed by Miller et al. (1995c).

The initialization survey spanned 14–16 August and included XBTs, XCTDs, and CTD data (Fig. 3a), sampled at a 24-km resolution in the east–

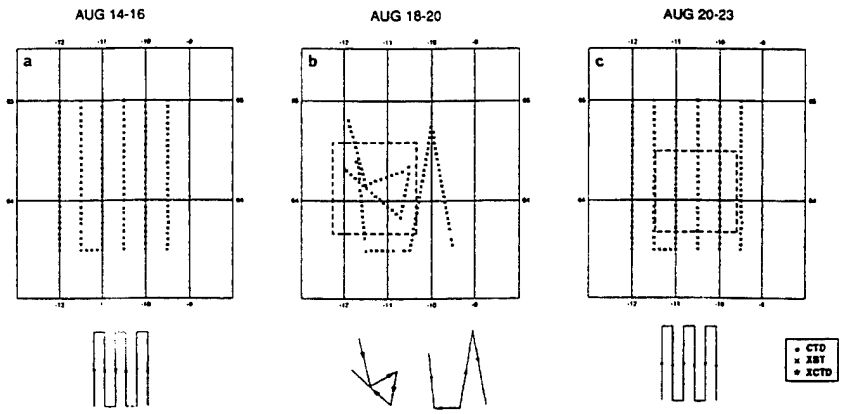

FIG. 3. Maps of the locations of the hydrographic surveys during the August 1993 cruise for (a) initialization survey, (b) zigzag survey, and (c) validation survey. The type of data acquired (XBT, CTD, XCTD) is indicated by a symbol. The path followed during the survey is sketched in the diagram beneath each figure. The subdomains in (b) and (c) are used for validation.

west direction and approximately a 7-km resolution in the north–south direction along track. The zigzag survey, from 18 to 19 August, consisted solely of XBTs in and around the western central part of the IFF (Fig. 3b). The validation survey, during 20–23 August, charted the same track as the initialization survey, albeit at a slower pace, because it included more CTDs among the hydrocasts (Fig. 3c). Once the data were collected and visually preprocessed (for obvious errors), the XBT data were supplemented with salinity data that were derived from a temperature–salinity (T–S) water mass model (Robinson et al. 1994). This water mass model was constructed during the cruise and used the CTD and XCTD salinities gathered in real time. As the water mass composition of each XBT was identified, salinity appropriate to that water mass, as measured on the cruise, was added to the XBT temperature information (with appropriate density constraints).

The synoptic observations for the three surveys are summarized in Fig. 4 in terms of temperature maps near the surface (25 m), upper water column (125 m), and deeper water column (level 4). The deeper map was prepared for assimilation in, and evaluation of, the dynamical model that uses a terrain-following ("sigma") coordinate system, which is explained in the next section. Sigma levels are not horizontal. The deeper water temperature map is predominantly located between 200 and 300 m (~220 m, but not exactly), but with a slope downward to the northeast.

The time-dependent objective analyses used an isotropic autocorrelation function of the form

$$C(r,\delta t)=\left[1+\left(\frac{r}{a}\right)^2\right]e^{-\frac{1}{2}\left(\frac{r}{b}\right)^2}e^{-\frac{1}{2}\left(\frac{\delta t}{c}\right)^2}+\sigma^2\delta_{ij}. \qquad (1)$$

Here r is a spatial lag vector having a magnitude of

$$r=\left[\left(x_i-x_j\right)^2+\left(y_i-y_j\right)^2\right]^{\frac{1}{2}},$$

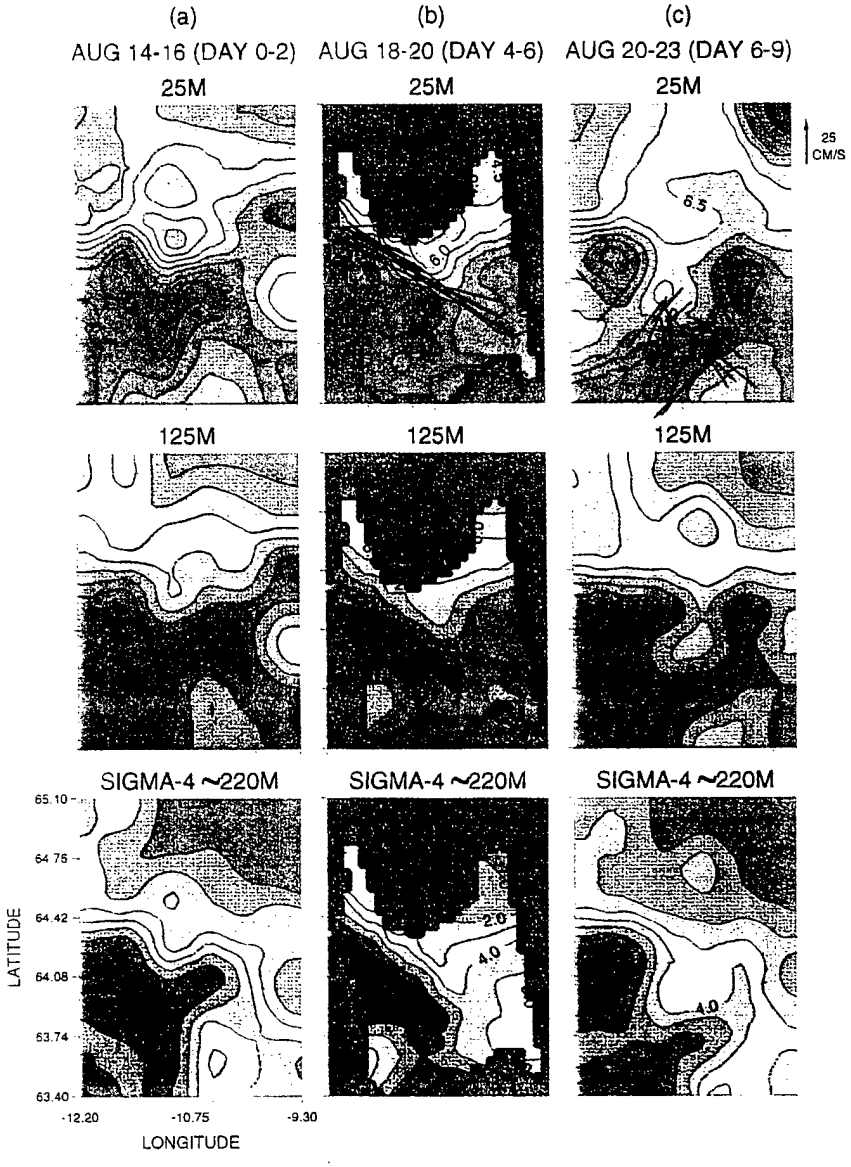

FIG. 4. Observed temperature, mapped by objective analysis, from the (a) initial survey, (b) assimilating zigzag survey, and (c) validating survey at (top) 25 m, (middle) 125 m, and (bottom) the sigma-coordinate level that varies from a 180- to a 300-m depth. At 25 m, the contour interval is 0.5°C. At 125 m and at sigma 4 (~220 m), the contour interval is 1°C. Surface drifter velocity observations (inferred from 12-h displacements, drogued to a 15-m depth) are shown for 18 and 19 August on the zigzag survey and for 21 and 22 August on the validation survey.

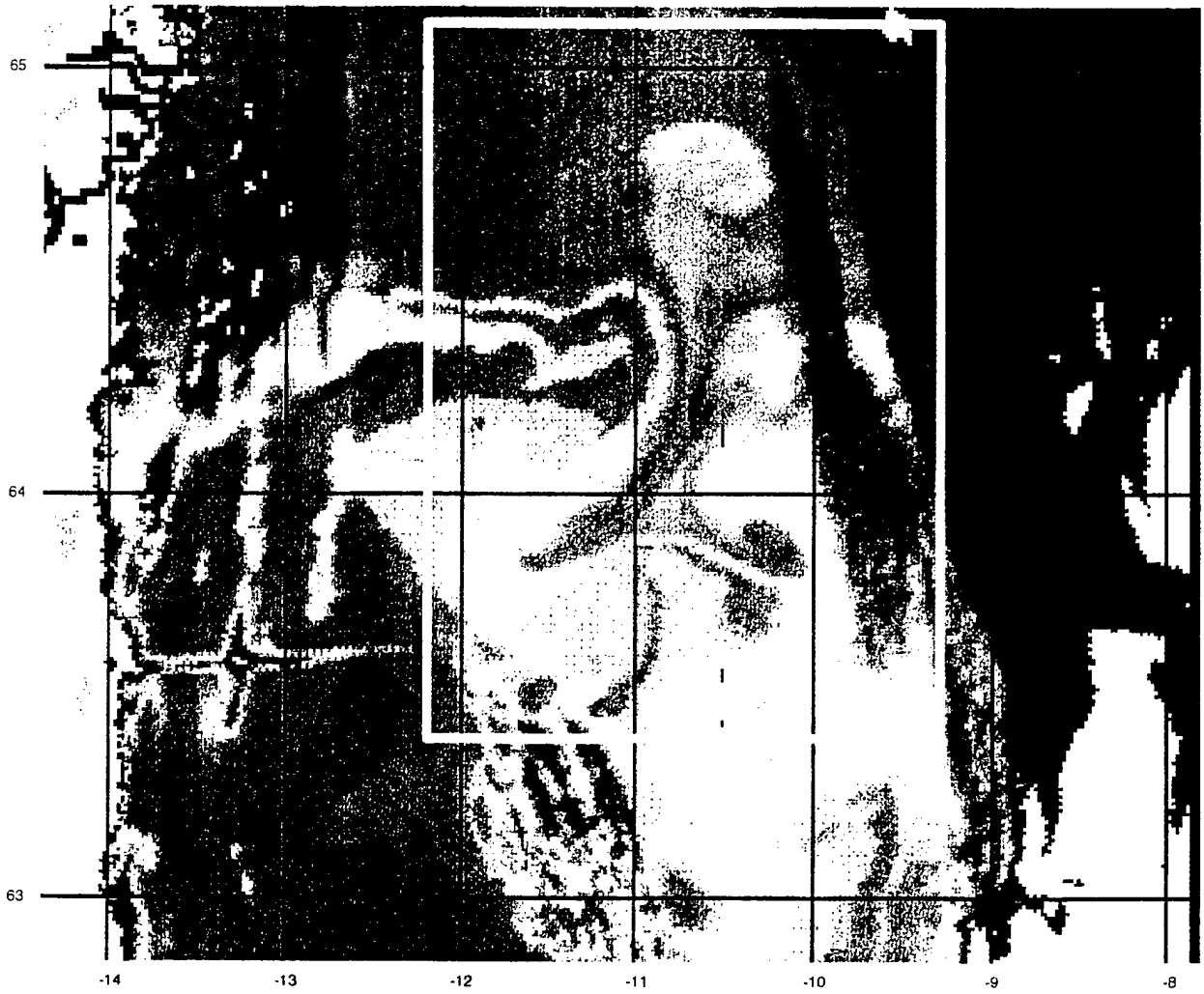

FIG. 5. Satellite infrared (channel 4 of AVHRR) image for 1431 UTC 22 August 1993. White and blue areas indicate clouds, pink areas cooler water, and green areas warmer water. The PE forecasting domain is traced in the image. Part of the coast of Iceland is delineated in the upper-left corner.

and

$$\delta t = t_i - t_j$$

is the temporal lag, a is the correlation zero crossing, b is the spatial decorrelation scale, c is the temporal decorrelation scale, σ^2 is the noise variance, and δ_{ij} is the Kronecker Delta ($\delta_{ij} = 1$ when $i = j$; otherwise, $\delta_{ij} = 0$). The value of these parameters used here are $a = 60$ km, $b = 40$ km, $c = 4$ days, and $\sigma^2 = 0.1$. Although it is generally necessary to take anisotropy into account in the vicinity of a jet, the dense data coverage allowed the use of an isotropic correlation function. In cases with dense sampling, the objective analysis scheme acts as a simple interpolator. The maps are for the central day of each survey, that is, 15, 19, and 22 August. Since the zigzag survey did not cover the entire domain, the maps of Fig. 4b are masked where the expected error of the analysis exceeds 25%. The near-surface maps also present surface drifter measurements of near-surface velocity; the drifters were drogued to provide the velocity at a 15-m depth.

In Fig. 4b, there are two clusters of 6-h displacement tracks for 18 and 19 August, and in Fig. 4c there are two clusters of 6-h displacements for 21 and 22 August. The drifters were launched as clusters, as opposed to being more widely dispersed, in order to investigate the dispersion about a center of mass and to provide information regarding divergence, convergence, vorticity, etc. By preceding the launch of the drifters with the first hydrographic survey, the drifters were able to be located close to the frontal axis in the most interesting location.

Near the surface and in the upper water column, the frontal and eddy fields are quite similar. However, there are distinct differences at depth in the central and eastern regions of the domain. Note that the inlet position of the front on the western boundary is nearly stationary throughout the experiment. On 15 August (Fig. 4a), the IFF was oriented eastward in a distinct meander pattern with a crest at about 11.5°W longitude and a trough at about 11°W. In the east, in the upper ocean (Fig. 4a; 25, 125 m), the flow broadens and bifurcates around a pair of eddies only partially contained within the domain. In the deep ocean, the front flows to the south, where it exits the domain. The general orientation and location of the deep front remained constant throughout the experiment but was accompanied by vigorous meandering (Figs. 4a,c at ~220 m). The upper frontal system evolved rapidly and changed qualitatively between each survey. By 19 August (Fig. 4b; 25, 125 m), the meander had disappeared, and the straightened frontal stream had shifted to a southeastward orientation in the western domain and a northeastward orientation in the eastern domain. However, only 3 days later, on 22 August (Fig. 4c; 25, 125 m), the dominant synoptic feature was a large cold intrusion or deep-sock meander, which had developed in the center of the domain. The center of the intrusion is shifted about 0.5° of longitude westward at 25 m relative to 125 m, and the near-surface meander is surrounded by a pair of strong, warm eddies. The drifter observations generally affirm the structure of the feature, flowing southwestward along the western border on 21 August followed by an eastward flow along the base on 22 August with a subsequent entrainment in the southward branch of the bifurcating flow. The satellite-observed sea surface temperature (Fig. 5) confirms unambiguously the existence of the deep-sock, or hammerhead, nonlinear meander.

4. Forecast methodology

The Harvard Ocean Prediction System (HOPS) is an integrated system of software developed in general for producing interdisciplinary oceanic field estimates, including nowcasts, forecasts, and data-driven simulations from a variety of data types and databases (Harvard Group 1994; Robinson 1993; Robinson et al. 1994). The general configuration is shown schematically in Fig. 6. It is a flexible, portable system whose modularity facilitates efficient configuration for specific applications. For the real-time operational forecasts aboard the R/V *Alliance* in August 1993 the configuration included modules for hydrographic data analysis; Lagrangian drifter analysis; objective analysis; optimal interpolation; climatology, correlation statistics, and a feature model for the IFF frontal current; primitive equation dynamics; and visualization. The Geophysical Fluid Dynamics Laboratory primitive equation model (Bryan and Cox 1967; Semtner 1974) provides the basic integration algorithm for the open boundary PE model used for HOPS. The PE open boundary conditions, subgrid-scale physics, and

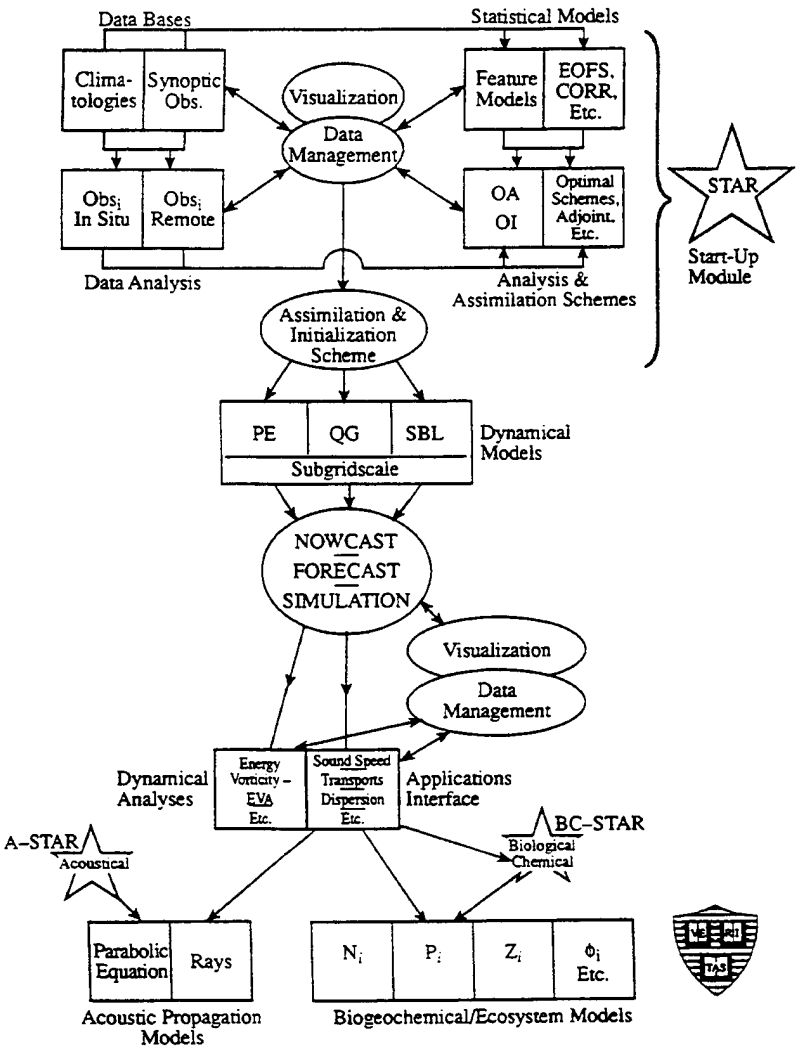

FIG. 6. Schematic of HOPS, the Harvard Ocean Prediction System.

bottom topographic treatment via hybrid coordinates were developed at Harvard; Spall and Robinson (1989) present the documentation and calibration. The PE integration algorithm has been modularized, and the pressure gradient algorithm replaced by one that maintains accuracy and efficiency in the presence of very steep and tall topography (Lozano et al. 1994).

The hybrid coordinate system consists of level surfaces in the upper ocean down to a prescribed depth below which a terrain-following sigma coordinate system is used. Sigma coordinates are gradually influenced by the shape of the bottom and a level sigma surface coincides with the bottom at the bottom. The PE model was set up with five "levels" in the vertical, horizontal surfaces at 25, 75, and 125 m and sigma surfaces located predominantly at ~220 and ~350 m, but with a pronounced downward slope localized in the northeast corner and a slight slope downward in the southeast corner. The horizontal resolution was 5 km, and the time step was 30 min. The subgrid-scale dissipation was accomplished by a Shapiro filter of order 4 applied five times each time step to the momentum and temperature equations. This is a weak filter, and for short forecasts there is little sensitivity to a reasonable range of filter parameters.

The PE model forecasts were driven by initial conditions, boundary conditions, and updating. The regional fields, as part of a larger-scale circulation system, evolved via internal dynamical processes. Local direct atmospheric forcing was neglected in the PE forecasts, which is an approximation that was consistent with the light and nearly constant winds experienced. Hydrographic data provide temperature and salinity directly for assimilation, and geostrophic computations provide the zero-depth-average internal velocity mode. The depth-averaged velocity, the barotropic or external mode, was inferred from geostrophy plus surface drifter information, which became available first on 18 August. The measured barotropic mode implied a surface geostrophic velocity that was 1.25 times the value of the surface value calculated relative to the bottom, which had been used prior to the availability of float data.

We term our general shipboard methodology to build and maintain a synoptic description of an oceanic region, primarily using in situ data obtained by the ship itself as it moves around the forecast region, as "sequential updating." A subdomain of the entire region is first analyzed when sufficient data have been obtained to make a reasonable nowcast. With a dedicated research vessel taking hydrographic observations with a mix of CTDs and expendable probes, this is typically 1 day's (24 h) worth of data. Given the differences between oceanographic and atmospheric event scales, 1 day for the ocean is comparable to 6 h for the atmosphere. When the first subdomain data are available, the entire domain is initialized, using in the data-empty region elements from the regional historical synoptical database, for example, a gridded climatology and/or feature models representing typical synoptic coherent structures. On successive days, as new subdomain datasets become available, they are assimilated via optimal interpolation into nowcasts. In this way, the entire domain is built up, with data being assimilated and evolving as synoptically as possible. When data have been collected over the entire domain, meaningful forecasting can begin. As the ship continues to operate in the region, the sequential assimilation procedure is continued whenever sufficient data are obtained over a subdomain to make updating meaningful. This methodology allows for initial analysis and nowcasting as soon as is possible.

The specific initialization and assimilation strategy for this experiment was as follows. We designate 14 August as day 0. The initialization survey took 3 days to accomplish (day 0, 1, 2) as the ship moved from east to west. The model was first initialized on day 0, with the strip (or slab) of data available in the eastern third of the domain. In the central and western areas of the domain, initialization consisted of a feature model representation of the frontal fields along the mean east–west axis of the stream, with estimated mean stratification to the north and south. The feature model is explained in the next section. When the central strip of data became available for day 1, it was assimilated via optimal interpolation, as was the day 2 data. Thus, the forecast domain was built up by a process of initialization on day 0, followed by two cycles of intermittent optimal interpolation on days 1 and 2. The field estimates from melded data and dynamics on days 0, 1, 2 we designate as nowcasts. The forecast carried out from this buildup process is designated as F2 (the last day of data assimilation). Zigzag survey data became available on day 5. The forecast carried out with the assimilation of this data is designated as F5. The OI assimilation weights were based primarily on the three-dimensional expected error distribution of the objectively analyzed (OA) maps of the data. The minimum observational error was 0.1, which was taken to correspond to an observational weight of 0.9. The OA

maps then produced the data weights to estimate the field $F_{est} = W_o F_{obs} + W_f F_{forecast}$, and the forecast weight was simply $W_f = 1 - W_o$. For F5, the zigzag data were treated as a damped assimilation and ramped up and down in time with maximum weights of 0.4 on day 4, 0.8 on day 5, and 0.4 on day 6. The open boundary conditions were, as usual, specified as inflow and outflow, with temperature, salinity, and tangential velocity specified on the inflow (Spall and Robinson 1989). During the nowcasts and forecasts, all boundary conditions were persisted except during an assimilation cycle. Although the zigzag survey maps (Fig. 4b) are masked at 25% error, the assimilation of the survey was carried out over the entire domain, including boundary updating. Development of the technical details for a successful methodology of east–west domain buildup with OI data assimilation was carried out via an Observation System Simulation Experiment (OSSE) reported by Robinson et al. (1994) based on data from a 1992 cruise to the IFF (Poulain 1992; Miller et al. 1995a).

Real-time operational nowcasts and forecasts of 7-day duration were issued on 16, 17, 19, 20, 21, and 23 August and delivered to the scientist-in-charge of the R/V *Alliance*. Those at-sea nowcasts and forecasts were used to determine existing conditions and evaluate positioning for upcoming work. Though not presented here, the forecasts are all similar to either F2 or F5 described above and discussed in the next section except for the final forecast that assimilated some validation survey data. The forecasts were carried out on two SUN SPARC-10 workstations brought aboard the R/V *Alliance* from Harvard University. The hydrographic data were collected, calibrated, and quality controlled by the SACLANTCEN scientific and technical group and then transferred to the Harvard modeling group. Drifter locations were obtained daily from Argos. The data were available from the SACLANTCEN group within 8 h of being collected, and subsequent processing for modeling work was completed within the next 3–12 h. The processing could be a lengthy procedure due to the quantity of data and the complexity of dynamical features contained therein. The average forecast took from 20–40 min on the SPARC stations for forecasts of 1–2 weeks duration.

5. Forecasts

Results for the nowcasts of days 0 and 2, F2 forecasts for days 5 and 8, and the F5 nowcast for day 5 and forecast for day 8 are presented in Figs. 7, 8, and 9, respectively. In each case, the temperature nowcasts and forecasts are shown for the near-surface and upper-ocean horizontal levels (25 m, 125 m) and the deeper sigma model level 4, predominantly located at 200–300 m, to facilitate comparison with the observations presented in Fig. 4. The predicted surface velocity vectors are overlaid on the near-surface temperatures.

a. Nowcasts for 14 and 16 August (days 0, 2)

Looking first at the nowcasts, day 0 (Fig. 7a) depicts the dynamically adjusted feature model initialization in the western and central domains, melded with the initialization via observations in the eastern domain. In this case, the feature model was constructed from a set of pseudo-observations. From the true observations in the eastern domain, a typical Atlantic water CTD cast and a typical Arctic water CTD cast were constructed, which were then used to construct a "pseudodataset" for central and western regions that had not yet been sampled. The axis of the front was located in a climatological mean position and a typical synoptic frontal width specified by including an appropriate distribution of pseudodata, which were then objectively analyzed over the entire domain for the day 0 nowcast initialization. A similar procedure was used for the day 1 nowcast.

Our use of feature models, in this region, for the representation of synoptic structures from sparse data, dates back to 1988 (Denbo and Robinson 1988b). While the chosen feature models for this work are semianalytical, digital feature models for the regional structures (Bennett et al. 1992) also exist. By combining the real-time observations with analytical models, an accurate picture of synoptic conditions can be generated.

The day 2 nowcast (Fig. 7b) has assimilated, via intermittent optimal interpolation in three daily cycles, the entire initialization survey dataset. It represents a field estimate in which synoptic data have been assimilated synoptically, dynamically adjusted, dynamically interpolated, and dynamically extrapolated. It should be compared with the objective analysis for the central day of the survey (Fig. 4a). Although a time-dependent OA was used, since every region of the domain was sampled only once, the full domain maps for day 0, 1 (not shown) are essentially identical to the day 2 map (Fig. 4a). What differs from day to day are the maps of expected error of the analyses: The OA and nowcast estimates of Figs. 4a and 7b are similar, but there are significant differences. In the nowcast, at 25 m, the meander in the west has already partially

collapsed, and at 125 m the meander crest has smoothed, and the trough has weakened and propagated westward. The deeper-level estimates at ~220 m do not noticeably differ. We believe that these dynamical adjustments are real and that the nowcast estimate based on synoptically assimilated data melded with dynamics provides the most realistic picture of the frontal system.

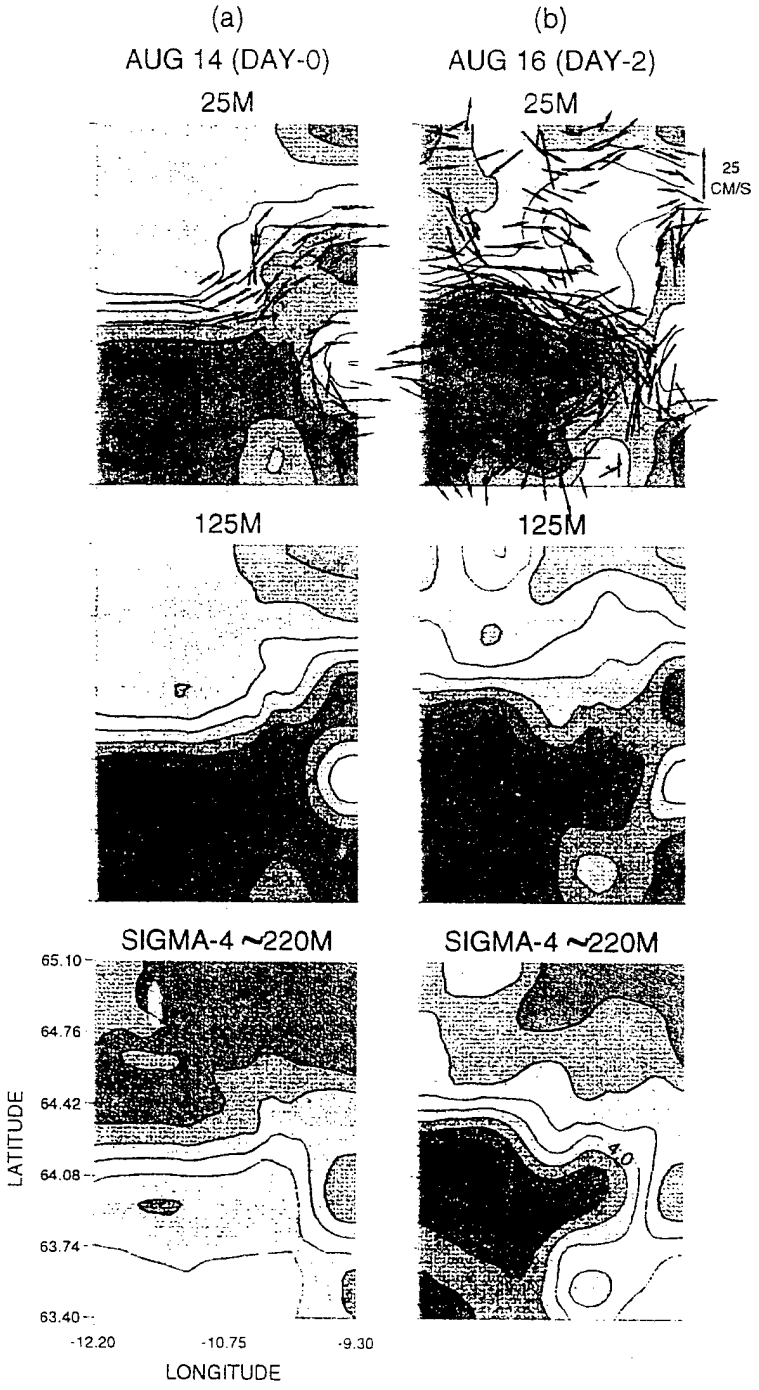

FIG. 7. The F2 nowcasts of temperature for (a) 14 August and (b) 16 August from the PE model, which assimilated data through 16 August, together with a feature model of the IFF. The velocity field for the top layer is also shown, otherwise plotted as in Fig. 4.

b. F2 forecasts and F5 nowcast for 19 August (day 5)

The F2 forecasts shown in Fig. 8 are regarded as initialized by the day 2 nowcast, and thus, the day 5 forecast of Fig. 8a is referred to as a 3-day forecast, and the day 8 forecast of Fig. 8b as a 6-day forecast. Evaluation of the 3-day forecast is possible within the masked region of Fig. 4b. The dynamics have successfully predicted the straightening and southward reorientation of the front in the western domain at all levels. The general northeastward orientation in the eastern domain at 25 and 125 m is also indicated in the forecast field, but at 25 m the prediction includes an unobserved meander pattern, which may well be due to the persistence of the day 2 boundary conditions on the eastern boundary. In the deeper ~220-m level, the persisted southern boundary condition is apparently causing local distortions and features. It is interesting to compare the F2, day 5 forecast (Fig. 8a) with the F5, day 5 estimate (Fig. 9a). Since the F5, day 5 estimate (Fig. 9a) has assimilated the zigzag survey with strong weights within the unmasked region of Fig. 8b, the Fig. 9a maps cannot, of course, be compared to the Fig. 8b maps. It is, however, interesting to note the difference in eastern and southern boundary regions of Figs. 8a and 9a that occurs from boundary updating under the influence of the zigzag data.

c. F2 and F5 forecasts of 22 August (day 8)

The 6-day F2 forecast and the 3-day F5 forecast for 22 August are shown in Figs. 8b and 9b, respectively. In both cases, the dynamics have developed an intense cold intrusion as observed in the validation survey (Fig. 4c). In both forecasts, the southward penetration of the intrusion agrees with observations, but the center is located a little eastward of

the observations, especially F2. Both are colder than observed, and F2 is oriented southeastward of the observations, while F5 has a small eastward protrusion not in the data. The agreement of both forecasts at 125 m is remarkably good. The location of the feature in F5 is excellent, and the only noticeable difference from observations is a nonlinear distortion on the western flank of the meander. The F2 feature is slightly too cold and displaced eastward of the data. The agreement between the F2 and F5 forecasts and the deeper data is also very good. The main difference is the meander amplitude, which is largest in the data (Fig. 4c, ~220 m), less in F5 (Fig. 9b, ~220 m), and weakest in F2 (Fig. 8b, ~220 m), which also has a contaminated southern boundary condition. Qualitatively, the dynamical prediction of this rapid and energetic event is very successful. Next we attempt to quantify the evaluation.

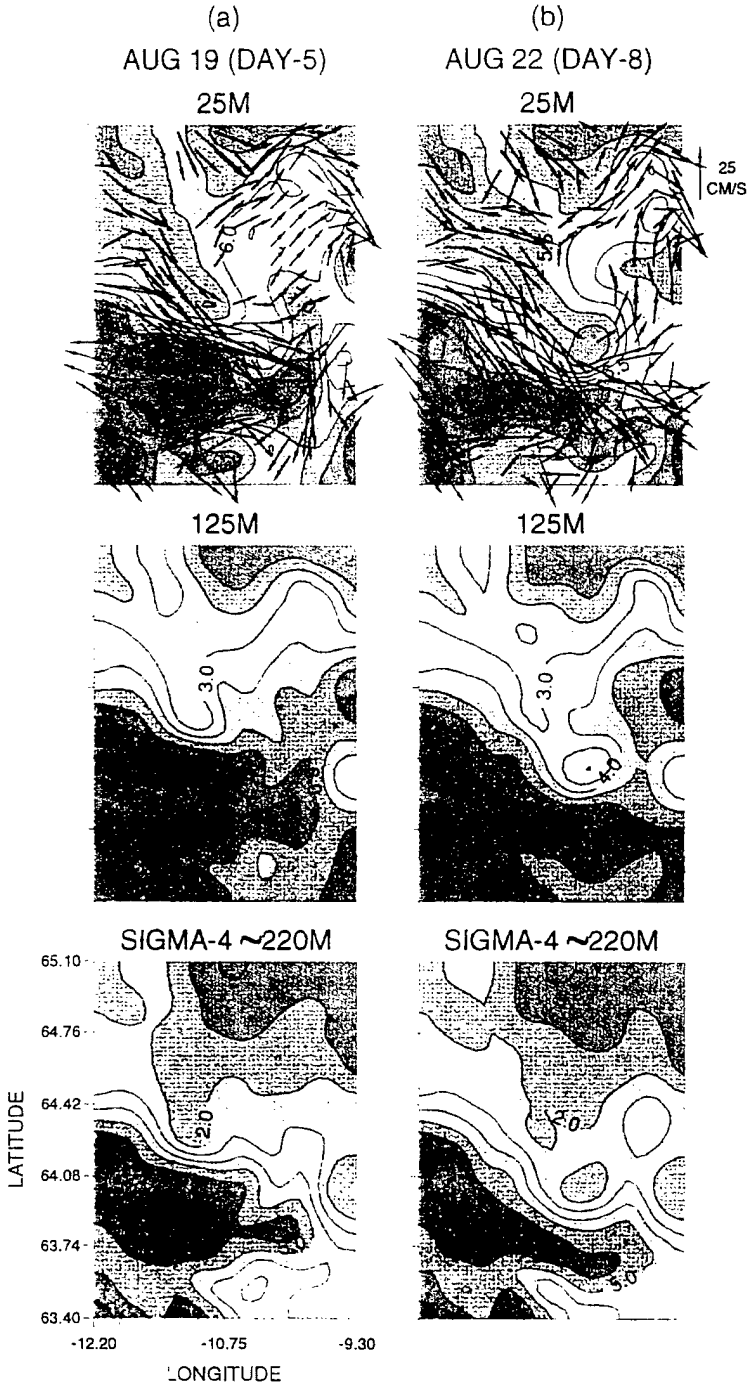

FIG. 8. The F2 forecasts of temperature for (a) 19 August and (b) 22 August for the PE model. Otherwise, as in Fig. 7.

6. Quantitative evaluation

Quantitative demonstrations of ocean mesoscale forecast skill are rare (e.g., see the special issue of *Oceanography* 1992, edited by R. A. Peloquin), and our results in this section are novel. Lynch (1995) provides an overview of the problem from a coastal ocean viewpoint. The sparseness of oceanic data, compared to atmospheric data, makes the verification problem generally very different. Often the lack of sufficient data requires one to devise clever measures of useful skill, such as mean frontal axis position error (Willems et al. 1994) or eddy-spawning event statistics (Robinson et al. 1989). Because we have such unprecedentedly complete initialization and validation information, we adopt the standard statistical validation measures, anomaly correlation coefficient and root-mean-square error (rmse),

$$\mathrm{ACC} = \frac{\langle T_p' T_p' \rangle}{\left(\langle T_p' \rangle \langle T_o' \rangle \right)^{1/2}}, \qquad (2)$$

and

$$\mathrm{rmse} \equiv \left\langle \left(T_p - T_o \right)^2 \right\rangle^{1/2}, \qquad (3)$$

where T_p' is the predicted temperature (with spatial mean removed), T_o' is the ob-

served temperature (with spatial mean removed), and the angle brackets denote averaging over a specified horizontal area. Note that T_p will apply either to the dynamical prediction or to the prediction of persistence of the initial state (i.e., last day of assimilation) against which all measures of quantitative skill will be referenced.

The data coverage, combined with our understanding of what events transpired during the three surveys, causes us to specify four distinct regions in which we can assess the quantitative skill. The first region is the entire model–observation domain (Fig. 2), which applies for F2 forecasting 7 days into the future. The second region is the zigzag area defined by the objective analysis error field (Fig. 4b); this region applies both to the validation data of F2 forecasting roughly 3 days into the future, and also for F5 forecasting 3 days into the future beyond the final assimilation of the zigzag data. The third region (subdomain A, Fig. 3b) is the dynamically interesting rectangular domain (12.2°–10.3°W and 63.7°–64.6°N), which surrounds the southeastward current that was observed to develop from the initial to the zigzag survey. The fourth region (subdomain B, Fig. 3c) is an 85-km-square domain (11.2°–8.3°W and 63.7°–64.5°N), covering the deep-sock meander that evolved from the zigzag survey to the third survey.

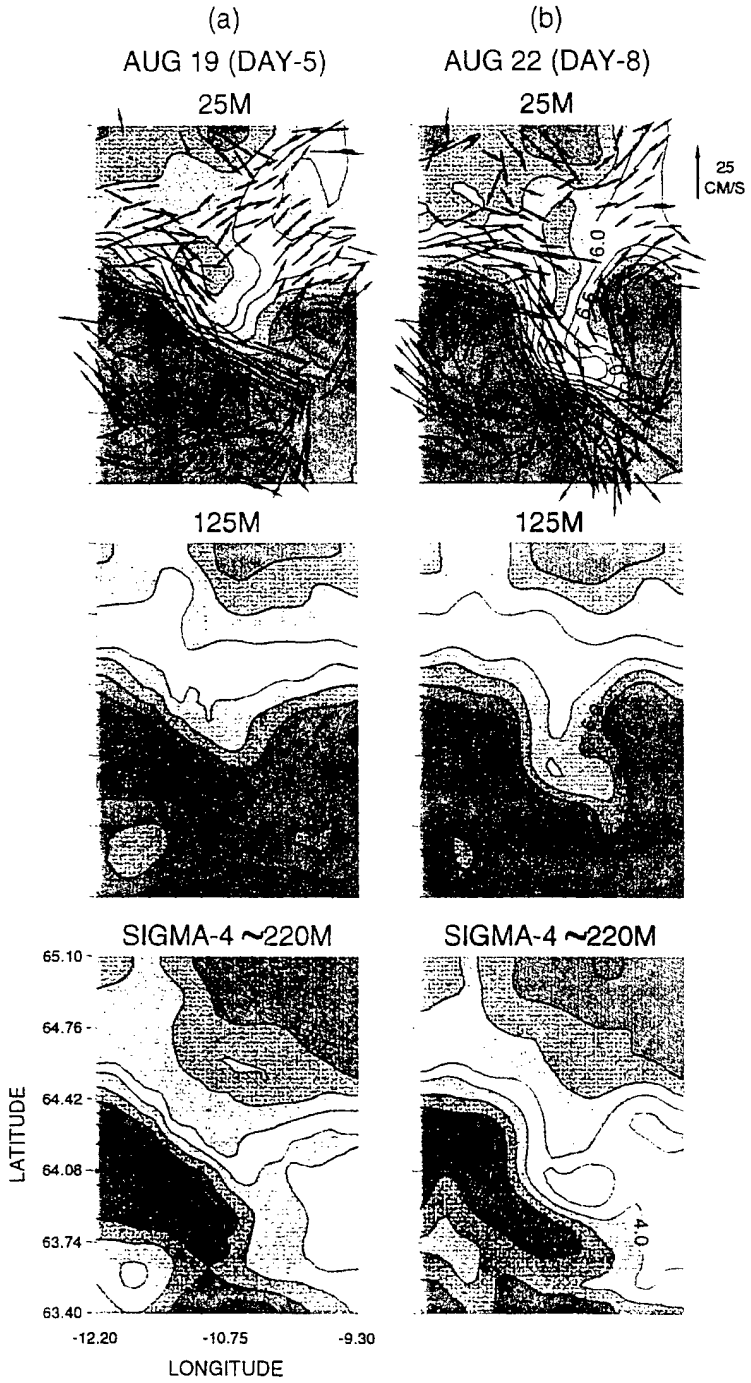

FIG. 9. The F5 (a) nowcast of temperature for 19 August and (b) forecast for 22 August for the PE model, which assimilate all data through 19 August, otherwise as in Fig. 8.

Although data was assimilated into the forecasts when acquired, we will treat the data that is used for validation as synoptic and assign representative central dates, namely 19 August for the zigzag survey (acquired 18–19 August) and 22 August for the validation survey (acquired 20–23 August).

In the previous section, we have discussed the significant qualitative forecast skill of the PE model. We therefore anticipate that we should attempt to account for forecasting phase errors, both in space and time, in order to uncover additional quantitative skill information. To reveal potential phase errors in time, we plot the skill scores (for correlation coefficient and the rmse) between each day of the forecast and the observations on the single day of validation (cf. Glenn and Robinson 1995; Miller et al. 1995b). Ideally, the skill should reach a maximum for the forecast day corresponding to the representative central date of the validating survey. To reveal potential phase errors in space, we shift the model prediction (translate the model grid) in both hori-

zontal directions and locate the maximum skill scores. These views of the relation between forecast and observations allow us to identify potential inadequacies in the time evolution of model dynamics, in the sense that, for example, a day $(N+2)$ forecast might be a superior predictor of day (N) observations, indicating that the model eddy features mature too slowly in time or that the fields develop, for example, too far downstream but with accurate spatial fidelity. The treatment of the spatial phase error is fairly crude, as it does not take into account possible pattern rotation, strain, or dilation.

As implied above, the three surveys provide two possibilities for F2 verification and one for F5. We now discuss these in turn.

a. F2 14–16 August assimilation/18–19 August verification

Table 1 shows the difference between the forecast skill and skill of persistence. A positive ACC difference (or a negative rmse change) indicates higher skill for the forecast. Due to the existence of the front, correlations remain high even for persistence forecasts (e.g., typical values of the ACC exceed 0.6 for either model forecasts or persistence of day 0). It should be noted that even a slight improvement in ACC for a forecast can explain a fair percentage of additional pattern variance of the field. For example, if a forecast field has ACC = 0.85, representing an increase of 0.10 over a persistence forecast ACC = 0.75, 16% additional variance of the pattern of the field has been predicted, which is useful. Root-mean-square error, which gives a direct measure of the amplitude discrepancies between forecast and observed, is shown in the tables as a normalized quantity (although it is plotted in subsequent figures in dimensional units).

The most important feature seen in the 18–19 August zigzag survey is the reorientation of the IFF current to a southeastward direction. Table 1 shows that, relative to persistence of the synoptic fields for 14–16 August, the F2 forecast correlates better than the persistence forecast at the top level (25 m) when verifying in the zigzag area. The remaining skill scores in the other levels are inferior to persistence. If we redirect our attention to the region surrounding the southeastward IFF current (subdomain A), we find (Table 1) that the F2 forecast correlates better than persistence at levels 1, 3, and 4. Level 4 also exhibits a reduced rmse relative to persistence. We did not attempt to account for phase errors in space for this case, since it was evident that the southeastward current developed at the correct location in the forecast.

b. F2 14–16 August assimilation/20–23 August verification

Validating F2 as a 6-day forecast, we found little evidence (Table 2) for quantitative skill when considering the entire model region as the domain of interest. Although a slight reduction in rmse was observed for level 4, the remaining levels all fared poorly compared to persistence in the full domain. In subdomain B, centered on the developed deep-sock meander, the forecast reveals some quantitative skill for both level 4 and level 5 (Table 2), as measured by our defined correlation measure. However, as noted above, the 7-day F2 forecast

TABLE 1. Primitive equation case F2 forecast skill vs persistence.

Assimilating 14–16 August/predicting 18–19 August				
	Zigzag area		Subdomain A	
Temperature at	ACC change	Rmse change	ACC change	Rmse change
25 m	+0.079	+15%	+0.042	+13%
75 m	−0.089	+23%	−0.013	+22%
125 m	−0.042	+11%	+0.005	+10%
sigma 4	−0.030	+5%	+0.025	−2%
sigma 5	−0.083	+30%	−0.050	+16%

TABLE 2. Primitive equation case F2 forecast skill vs persistence.

Assimilating 14–16 August/predicting 20–23 August				
	Full domain		Subdomain B	
Temperature at	ACC change	Rmse change	ACC change	Rmse change
25 m	−0.307	+74%	−0.202	+58%
75 m	−0.119	+41%	−0.218	+73%
125 m	−0.065	+28%	−0.029	+27%
sigma 4	0.000	−3%	+0.101	−20%
sigma 5	−0.018	+8%	+0.033	−10%

successfully forms the cold intrusion feature and, thus, provides a much more useful field estimate for applications than does persistence, although this usefulness is not able to be quantified by our present measure.

c. F5 14–19 August assimilation/20–23 August verification

The quantitative forecast skill for F5 is presented in Table 3, and the results are impressive. When validating over the entire zigzag region, all model levels show increased skill relative to persistence, both in an increased correlation coefficient and in a reduced rmse. Focusing on subdomain B, surrounding the deep sock, Table 3 and Figs. 10 and 11 show that the skill levels drop a bit for the upper two levels but rise even higher for the deeper levels. It is clear that this forecast has substantial quantitative skill.

As discussed previously, the modeled deep-sock meander is in phase with the observed at depth (greater than 50 m) but occurs downstream of the observed near the surface. So we now account for this spatial disparity as a function of model level as shown in Table 4 and Figs. 10 and 11. The solid lines show the forecasting skill for each day of the forecast in subdomain B, validating for the 20–23 August survey. A forecast of persistence of the 18–19 August observations is indicated by the dashed line. The dotted line indicates the maximum skill of the spatially lagged 22 August forecast. For the top level (25 m), the maximum skill occurs when the forecast is shifted 10 km west and 5 km south (one model grid point equaling 5 km). For the 75-m layer, the maximum skill is obtained when shifting the model fields 10 km east and 10 km south, and at 125 m, the forecast must be shifted 10 km south. For the sigma coordinate layers, the shift is 5 km west, 10 km south, for level 4 and only 5 km south for level 5. The fact that all the spatial lags are 10 km or less reveals the high skill of this forecast. Thus, this analysis shows that the model field tends to be somewhat too "equivalent barotropic," in the sense that the observed field at 25 m develops upstream relative to the fields at depth, while the model field tends to develop in phase from top to bottom.

Skillful results were also obtained for upper water column flows using a quasigeostrophic forecast model (Miller et al. 1995b), although the QG model was unable to capture the sharp and narrow features of the hammerhead structure observed in the satellite map (Fig. 5) and PE forecast temperature field (Fig. 9). However, the QG model was validated against dynamic height rather than temperature as accomplished here; a direct comparison between forecast PE and QG current or dynamic height fields has yet to be carried out. But since both the PE and (flat bottom) QG models exhibited upper-ocean forecast skill, we note that topographic influence was minimal during the 3–4 days of the simulations because the modeled instability apparently was trapped in the upper part of the water column. Only the PE model was able to forecast the deep flows around the IFF with fidelity.

7. Discussion and conclusions

From 14–23 August 1993, there occurred in the meandering and eddying IFF system two rapid and en-

TABLE 3. Primitive equation case F5 forecast skill vs persistence.

Assimilating 14–19 August/predicting 20–23 August				
	Zigzag area		Subdomain B	
Temperature at	ACC change	Rmse change	ACC change	Rmse change
25 m	+0.023	−3%	−0.039	−1%
75 m	+0.022	−5%	+0.019	+1%
125 m	+0.044	−11%	+0.060	−12%
sigma 4	+0.072	−21%	+0.100	−27%
sigma 5	+0.078	−30%	+0.160	−43%

TABLE 4. Primitive equation case F5 space-lagged forecast skill vs persistence.

Assimilating 14–19 August/predicting 20–23 August				
	Spatial lag		Subdomain B	
Temperature at	East–west lag (km)	North–south lag (km)	ACC change	Rmse change
25 m	+10	+5	+0.140	−17%
75 m	−10	+10	+0.142	−7%
125 m	0	+10	+0.146	−18%
sigma 4	+5	+10	+0.139	−39%
sigma 5	0	+5	+0.187	−50%

ergetic synoptic dynamical events controlled by intermittent burst baroclinic instability. The frontal jet straightened and shifted and then developed a nonlinear hammerhead meander with Arctic water intruding deeply southward. Real-time operational nowcasting via intermittent optimal interpolation assimilation into a primitive equation model, fused the direct stream of hydrographic data as it became available with a feature model and climatology-based representation of the system. This approach provides a powerful and efficient method to generate what we believe to be a very accurate synoptic description of a region as data are collected. This approach could be further improved by using a more sophisticated assimilation methodology. Forecasts very successfully evolved these features dynamically. Statistical quantities that were introduced to quantify forecast skill (anomaly correlation and rmse) indicate that primitive equation dynamical forecasts significantly exceed persistence for a few days. We believe that these methods will prove generally useful as ocean forecasting progresses and can be further developed to allow for better treatment of phase errors. This is important because small spatial scales and the existence of many structures and features makes quantitative verification of ocean mesoscale variability forecasting challenging.

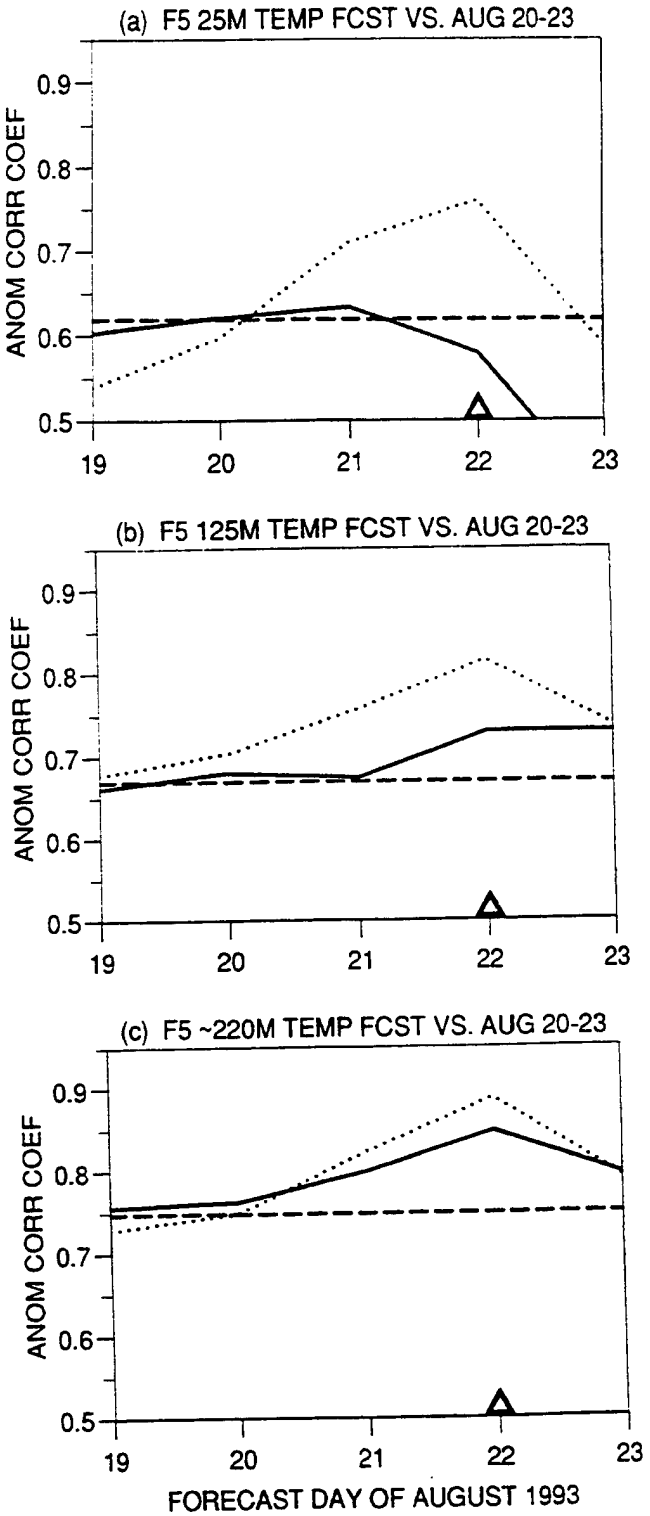

The capability of accurate and efficient real-time nowcasting and forecasting at sea has important implications for ocean science, technology, operations, and management. It makes possible a knowledge of present and future realistic oceanic fields with minimal observational resources. The dataset itself, designed and acquired for a forecast experiment, is of unprecedented quality as a database for regional ocean forecasting research, including observation system simulation experiments to determine minimal resource requirements for field estimates of predetermined accuracy. The data are available as a useful evaluation and verification resource to the ocean forecasting community.

Acknowledgments. The observations discussed in this work were obtained via the skilled data acquisition and processing abilities of the CTD/XCTD/XBT support staff of SACLANTCEN's Applied Oceanography Group, Ocean Engineering Department, and Digital Computer Department, and the captain and crew of the R/V *Alliance*. The Harvard group wishes to thank the following individuals at Harvard University for their efforts in the de-

FIG. 10. Anomaly correlation coefficient between each day of forecast temperature and the observations of 20–23 August for case F5 (14–19 August assimilation) at (a) 25 m, (b) 125 m, and (c) sigma level 4, in the specified area subdomain B (11.2°–8.3°W and 63.7–64.5N). The dashed line corresponds to persistence of observations for 18–20 August. Solid line corresponds to the real-time forecast, which ideally should be a maximum on 22 August (indicated by the triangle). The dotted line corresponds to the spatially lagged forecast that maximizes the correlation on 22 August, as described in text. At 25 m, the maximum correlation occurs when the forecast field is shifted 10 km west and 5 km south, at 125 m, shifted 10 km south, and at sigma 4, shifted 5 km south.

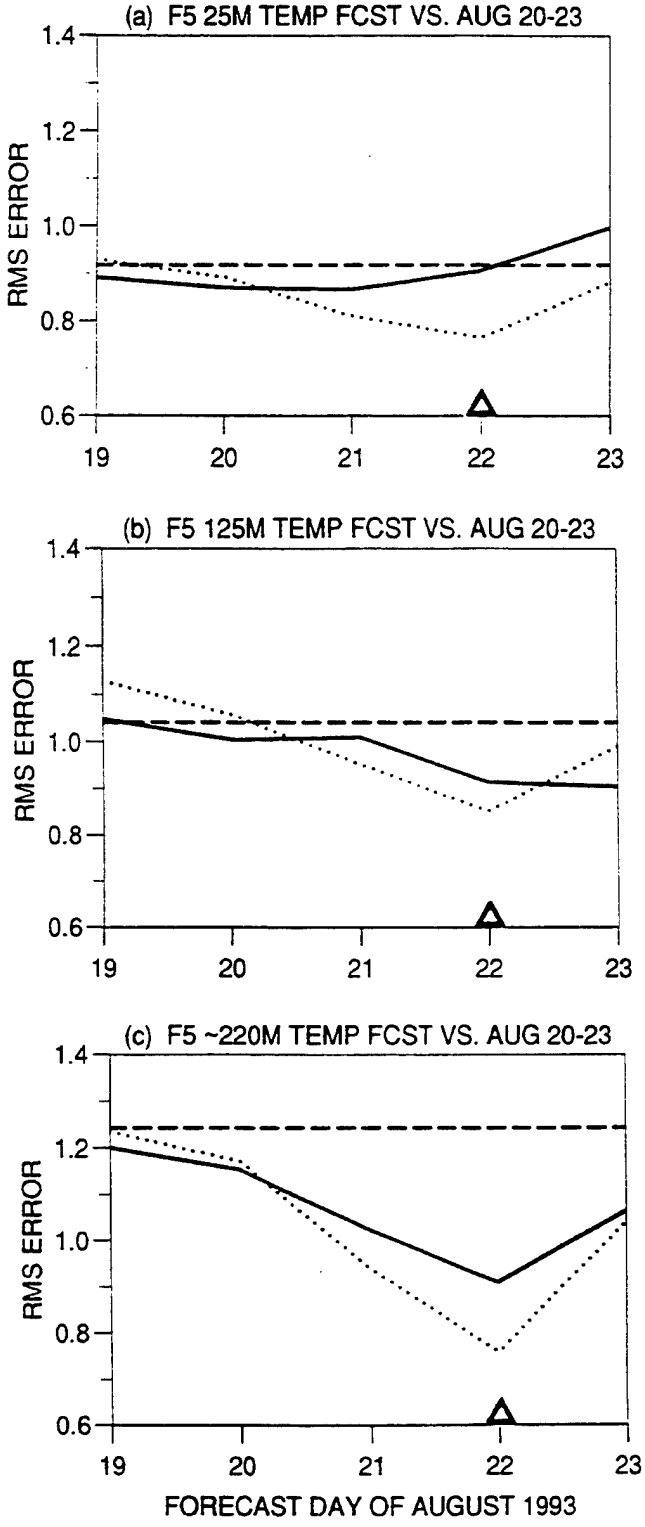

FIG. 11. As in Fig. 10 but for rmse.

velopment and setup of the models used during this experiment: Dr. Patrick J. Haley, Dr. Carlos Lozano, and Mr. N. Quinn Sloan III. Marsha Glass supplied invaluable logistical assistance. AJM was supported by SACLANTCEN during the data acquisition and forecast analysis stages of this work and is supported at SIO by NOAA Grants NA36GPO372 and NA47GPO188. The Fleet Numerical Oceanographic Center (FNOC) provided the NODDS products. This research was supported at Harvard University by the Office of Naval Research under Grants N00014-93-1-0577, N00014-90-J-1612, and N00014-91-J-1521.

References

Allen, J. T., D. A. Smeed, and A. L. Chadwick, 1994: Eddies and mixing at the Iceland–Faroes Front. *Deep-Sea Res.*, **41,** 51–74.

Bennett, T., Jr., J. Boyd, L. Knauer, G. Dawson, and W. Wilson, 1992: A feature model of the Iceland–Faeroe Front. *Mar. Tech. Soc. J.*, **26**(2), 44–52.

Bryan, K., and M. D. Cox, 1967: A numerical investigation of the oceanic general circulation. *Tellus,* **19,** 54–80.

Clancy, R. M., 1992: Operational modeling: Ocean modeling at the Fleet Numerical Oceanography Center. *Oceanography,* **5,** 31–35.

Denbo, D. W., and A. R. Robinson, 1988a: Harvard gapcasts; a progress report: Regional forecasting, processes and methodology in the Iceland–Faeroe Island gap. Part I: Data forecast and hindcast experiments. Reports in Meteorology and Oceanography: Harvard Open Ocean Model Rep., 32, 203 pp. [Available from Division of Applied Sciences, Dept. of Earth and Planetary Sciences, Pierce Hall, Harvard University, Cambridge, MA 02138.]

——, and ——, 1988b: Harvard gapcasts; a progress report: Regional forecasting, processes and methodology in the Iceland–Faeroe Island gap. Part II: GFD and process experiments. Reports in Meteorology and Oceanography: Harvard Open Ocean Model Rep., 33, 218 pp. [Available from Division of Applied Sciences, Dept. of Earth and Planetary Sciences, Pierce Hall, Harvard University, Cambridge, MA 02138.]

Dietrich, G., 1969: Atlas of the hydrography of the northern North Atlantic. Conseil International pour l'Exploration de la Mer. Service Hydrographie, Charlottenlund Slot, Denmark.

Durham, D. L., and J. K. Lewis, 1992: Introduction: Oceanic and atmospheric nowcasting and forecasting. *Mar. Tech. Soc. J.,* **29,** 3–4.

Fuglister, F. C., 1963: Gulf Stream '60. *Progress in Oceanography,* Vol. 1, Pergamon, 265–373.

Glenn, S. M., and A. R. Robinson, 1995: Verification of an Operational Gulf Stream Forecasting Model. *Quantitative Skill Assessment for Coastal Ocean Models, Coastal and Estuarine Studies,* Vol. 47, D. Lynch, Ed., Amer. Geophys. Union, 469–499.

Gould, W. J., J. F. Read, and J. Smithers, 1987: SEASOAR profiles in the Iceland–Scotland area, May 1987. Rep. 253, Inst. of Oceanogr. Sci., Wormley, England, 50 pp.

Hansen, B., and J. Meincke, 1979: Eddies and meanders in the Iceland–Faeroe Ridge area. *Deep-Sea Res.,* **26A,** 1067–1082.

Harvard Group, 1994: HOPS, the Harvard Ocean Prediction System. [Available from Division of Applied Sciences, Dept. of Earth and Planetary Sciences, Pierce Hall, Harvard University, Cambridge, MA 02138.]

Hopkins, T. S., 1991: The GIN Sea—A synthesis of its physical oceanography and literature 1972–1985. *Earth-Sci. Rev.,* **30,** 175–318.

Lai, C.-C. A., W. Qian, and S. M. Glenn, 1994: Data assimilation and model evaluation datasets. *Bull. Amer. Meteor. Soc.,* **75,** 793–809.

Lozano, C. J., P. J. Haley, H. G. Arango, N. Q. Sloan, and A. R. Robinson, 1994: Harvard coastal/deep water primitive equation model. Reports in Meteorology and Oceanography: Harvard Open Ocean Model Reports, 15 pp. [Available from Division of Applied Sciences, Dept. of Earth and Planetary Sciences, Pierce Hall, Harvard University, Cambridge, MA 02138.]

Miller, A. J., H. G. Arango, A. R. Robinson, W. G. Leslie, P.-M. Poulain, and A. Warn-Varnas, 1995a: Quasigeostrophic forecasting and physical processes of Iceland–Faeroe Front variability. *J. Phys. Oceanogr.*, **25,** 1273–1295.

——, P.-M. Poulain, A. R. Robinson, H. G. Arango, W. G. Leslie, and A. Warn-Varnas, 1995b: Quantitative skill of quasigeostrophic forecasts of a baroclinically unstable Iceland–Faeroe Front. *J. Geophys. Res.*, **100,** in press.

——, P. F. J. G. Lermusiaux, and P.-M. Poulain, 1995c: A 1.8-day topographic Rossby mode resonance trapped to the Iceland–Faeroe Ridge. Preprints, *10th Conf. on Atmospheric and Oceanic Waves and Stability,* Big Sky, MT, Amer. Meteor. Soc., 19–20.

Mooers, C. N. K., A. R. Robinson, and J. D. Thompson, 1986: Ocean prediction workshop 1986. A status and prospectus report on the scientific basis and the navy's needs. *Proc. Ocean Prediction Workshop,* Parts I and II, Cambridge, MA and Long Beach, MI, Institute for Naval Oceanography, NSTL, MS, 486 pp.

Niiler, P. P., S. Piacsek, L. Neuberg, and A. Warn-Varnas, 1992: Sea surface temperature variability of the Iceland–Faeroe Front. *J. Geophys. Res.*, **97,** 17 777–17 785.

Peggion, G., 1991: Diagnostic calculations for the reconstruction of environmental and acoustic conditions in the Iceland–Faeroe Ridge region during June 1989. SACLANTCEN SR-178, 65 pp. [Available from SACLANT Undersea Research Centre, 19138 La Spezia, Italy.]

Peloquin, R. A., 1992: The navy ocean modeling and prediction program. *Oceanography,* **5,** 4–8.

Perkins, H., 1992: Large-scale structure of the Iceland–Faeroe Front. SACLANTCEN SR-189, 40 pp. [Available from SACLANT Undersea Research Centre, 19138 La Spezia, Italy.]

Poulain, P.-M., 1992: Cruise report for R/V *Alliance* cruise: GIN92, Greenock-Liverpool, 13–29 October 1992. 29 pp. [Available from SACLANT Undersea Research Centre, 19138 La Spezia, Italy.]

——, 1993: Cruise report for R/V *Alliance* Cruise: GIN93, Wilhelmshaven-Bodo, 11–26 August 1993. 33 pp. [Available from SACLANT Undersea Research Centre, 19138 La Spezia, Italy.]

Read, J. F., and R. T. Pollard, 1992: Water masses in the region of the Iceland–Faeroe Front. *J. Phys. Oceanogr.*, **22,** 1365–1378.

Robinson, A. R., Ed., 1983: *Eddies in Marine Science,* Springer-Verlag, 609 pp.

——, 1992: Shipboard prediction with a regional forecast model. *Oceanography,* **5,** 42–48.

——, 1993: Physical processes, field estimation and interdisciplinary ocean modeling. Reports in Meteorology and Oceanography: Harvard Open Ocean Model Rep. 51. 80 pp. [Available from Division of Applied Sciences, Dept. of Earth and Planetary Sciences, Pierce Hall, Harvard University, Cambridge, MA 02138.]

——, S. M. Glenn, M. A. Spall, L. J. Walstad, G. M. Gardner, and W. G. Leslie, 1989: Forecasting Gulf Stream meanders and rings. *Trans. Amer. Geophys. Union,* **70**(45), 1464–1473.

——, and Coauthors, 1994: Real-time nowcasting and forecasting R/V *Alliance* GIN 93 Cruise 11–26 August 1993 operational forecasts and simulation experiments at sea. Reports in Meteorology and Oceanography: Harvard Open Ocean Model Rep. 50, XXX pp. [Available from Division of Applied Sciences, Dept. of Earth and Planetary Sciences, Pierce Hall, Harvard University, Cambridge, MA 02138.]

Scott, J. C., and N. A. Lane, 1990: Frontal boundaries and eddies on the Iceland–Faeroe Ridge. *Proceedings on Ocean Variability and Acoustic Propagation,* J. Potter and A. Warn-Varnas, Eds., Kluwer Academic, 449–461.

——, and A. L. McDowall, 1990: Cross-frontal cold jets near Iceland: In-water, satellite infrared and GEOSAT altimeter data. *J. Geophys. Res.*, **95,** 18 005–18 014.

Semtner, A. J., 1974: An oceanic general circulation model with bottom topography. Tech. Rep. 9, Department of Meteorology, University of California, Los Angeles, 99 pp.

Smart, J. H., 1984: Spatial variability of major frontal systems in the North Atlantic Norwegian Sea area: 1980–1981. *J. Phys. Oceanogr.*, **14,** 185–192.

Spall, M. A., and A. R. Robinson, 1989: A new open ocean, hybrid coordinate primitive equation model. *Mathematics and Computers in Simulation,* **31,** 241–269.

Willebrand, J., and J. Meincke, 1980: Statistical analysis of fluctuations in the Iceland–Scotland frontal zone. *Deep-Sea Res.*, **27A,** 1049–1066.

Willems, R. C., and Coauthors, 1994: Experiment evaluates ocean models and data assimilation in the Gulf Stream. *Trans. Amer. Geophys. Union,* **75,** 34.

[Reprinted from BULLETIN OF THE AMERICAN METEOROLOGICAL SOCIETY, Vol. 77, No. 2, February 1996]
Printed in U. S. A.